

## Article

# Mitochondrial Peroxiredoxin 3 Is Rapidly Oxidized and Hyperoxidized by Fatty Acid Hydroperoxides

Giuliana Cardozo<sup>1,2</sup>, Mauricio Mastrogiovanni<sup>1,2</sup> , Ari Zeida<sup>1,2</sup> , Nicolás Viera<sup>1,2</sup>, Rafael Radi<sup>1,2</sup>, Aníbal M. Reyes<sup>1,2,\*</sup>  and Madia Trujillo<sup>1,2,\*</sup> 

<sup>1</sup> Departamento de Bioquímica, Facultad de Medicina, Universidad de la República, Montevideo 11800, Uruguay

<sup>2</sup> Centro de Investigaciones Biomédicas, Universidad de la República, Montevideo 11800, Uruguay

\* Correspondence: marceloreyes@fmed.edu.uy (A.M.R.); madiat@fmed.edu.uy (M.T.)

**Abstract:** Human peroxiredoxin 3 (*HsPrx3*) is a thiol-based peroxidase responsible for the reduction of most hydrogen peroxide and peroxyxynitrite formed in mitochondria. Mitochondrial dysfunction can lead to membrane lipoperoxidation, resulting in the formation of lipid-bound fatty acid hydroperoxides ( $\text{LFA-OOHs}$ ) which can be released to become free fatty acid hydroperoxides ( $\text{fFA-OOHs}$ ). Herein, we report that *HsPrx3* is oxidized and hyperoxidized by  $\text{fFA-OOHs}$  including those derived from arachidonic acid and eicosapentaenoic acid peroxidation at position 15 with remarkably high rate constants of oxidation ( $>3.5 \times 10^7 \text{ M}^{-1}\text{s}^{-1}$ ) and hyperoxidation ( $\sim 2 \times 10^7 \text{ M}^{-1}\text{s}^{-1}$ ). The endoperoxide-hydroperoxide  $\text{PGG}_2$ , an intermediate in prostanoid synthesis, oxidized *HsPrx3* with a similar rate constant, but was less effective in causing hyperoxidation. Biophysical methodologies suggest that *HsPrx3* can bind hydrophobic structures. Indeed, molecular dynamic simulations allowed the identification of a hydrophobic patch near the enzyme active site that can allocate the hydroperoxide group of  $\text{fFA-OOHs}$  in close proximity to the thiolate in the peroxidatic cysteine. Simulations performed using available and herein reported kinetic data indicate that *HsPrx3* should be considered a main target for mitochondrial  $\text{fFA-OOHs}$ . Finally, kinetic simulation analysis support that mitochondrial  $\text{fFA-OOHs}$  formation fluxes in the range of nM/s are expected to contribute to *HsPrx3* hyperoxidation, a modification that has been detected in vivo under physiological and pathological conditions.

**Keywords:** peroxiredoxin; mitochondria; fatty acid hydroperoxide; lipid peroxidation; antioxidant systems; kinetics



**Citation:** Cardozo, G.; Mastrogiovanni, M.; Zeida, A.; Viera, N.; Radi, R.; Reyes, A.M.; Trujillo, M. Mitochondrial Peroxiredoxin 3 Is Rapidly Oxidized and Hyperoxidized by Fatty Acid Hydroperoxides. *Antioxidants* **2023**, *12*, 408. <https://doi.org/10.3390/antiox12020408>

Academic Editor: Jiankang Liu

Received: 26 December 2022

Revised: 19 January 2023

Accepted: 28 January 2023

Published: 7 February 2023



**Copyright:** © 2023 by the authors. Licensee MDPI, Basel, Switzerland. This article is an open access article distributed under the terms and conditions of the Creative Commons Attribution (CC BY) license (<https://creativecommons.org/licenses/by/4.0/>).

## 1. Introduction

In most mammalian cells, mitochondria are main sources of oxidizing species [1,2]. Among them, it forms different hydroperoxides such as hydrogen peroxide ( $\text{H}_2\text{O}_2$ ), peroxyxynitrite and either free or lipid-bound fatty acid hydroperoxides ( $\text{fFA-OOHs}$  or  $\text{LFA-OOHs}$ , respectively), many of which participate in cellular redox signaling pathways at low, physiological concentrations [3–5]. However, increased steady-state levels of these species can lead to mitochondrial dysfunction, cytotoxicity and several disease states [4,6–10]. Different peroxidases reduce hydroperoxides in mitochondria [11]. Peroxiredoxin 3 (Prx3) catalyzes the reduction of most of mitochondrial  $\text{H}_2\text{O}_2$  [12]. Furthermore, our previous work indicates that Prx3 is an efficient peroxyxynitrite reductase that represents, together with peroxiredoxin 5 (Prx5), the main target for peroxyxynitrite in mitochondria [13]. Both  $\text{H}_2\text{O}_2$  and peroxyxynitrite can lead to Prx3 inactivation due to peroxidatic cysteine ( $\text{Cys}_\text{P}$ ) hyperoxidation to sulfinic acid ( $\text{RSO}_2\text{H}$ ) or even to sulfonic acid ( $\text{RSO}_3\text{H}$ ), although the enzyme is considered to be less susceptible to this modification than other mammalian typical two cysteine peroxiredoxins (Prxs) such as Prx2 [13,14]. This was ascribed to a slower rate constant of resolution, i.e., change from the fully folded (FF) to locally unfolded (LU)

conformation followed by the formation of an inter-subunit disulfide with the so-called resolving cysteine residue (Cys<sub>R</sub>), in the case of Prx3 [13,15].

$\text{LFA-OOHs}$  can be produced non-enzymatically due to mitochondrial membrane lipoperoxidation processes, initiated by the reaction of different one-electron oxidants with polyunsaturated fatty acids (PUFA) such as linoleic acid (LA) and arachidonic acid (AA). Alternatively, enzymatic mechanisms can also lead to FA-OOHs formation [16,17]. In particular, the inner mitochondrial membrane is characterized by a high degree of unsaturation and is rich in phosphatidyl ethanolamine, phosphatidyl choline and cardiolipin, a phospholipid in which two phosphatidic acid groups are attached to a central glycerol molecule (Membrane composition varies among cell compartments and tissues. In rat liver inner mitochondrial membranes, phosphatidyl ethanolamine, phosphatidyl choline and cardiolipin represent 40%, 40% and 20% of total phospholipids, respectively [18]). The interaction of cardiolipin with cytochrome *c* leads to an increase in the peroxidase activity of the latter that promotes the oxidation of PUFA in the phospholipid [19]. Increased formation of oxidants and lipid peroxidation induces the activation of mitochondrial phospholipases, resulting in the release of the corresponding hydroperoxides ( $\text{fFA-OOHs}$ ) from oxidized membranes, which participate in physiological signaling cascades and in mitochondrial uncoupling [16,20–22]. Additionally,  $\text{fFA-OOHs}$  formed in the cytosol can diffuse into the mitochondria leading to changes in the membrane potential, release of cytochrome *c* and generation of further oxidative species [23]. Increased lipoperoxidation is a key participant in ferroptosis, an iron-dependent form of regulated cell death characterized by increased lipoperoxidation in cellular membranes [24] that may result in pathologies such as neurodegenerative diseases [25,26].

Both free and lipid-bound FA-OOHs are reduced to the corresponding alcohols by the selenocysteine-containing enzyme glutathione peroxidase 4 (GPx4) [27,28]. Indeed, homozygous GPx4 knock-out mice are not viable and cells lacking GPx4 activity die due to increased lipoperoxidation that is a hallmark of ferroptosis [29]. Although the enzyme is expressed as cytosolic, mitochondrial and nuclear isoforms, inactivation of mitochondrial GPx4 alone allowed normal embryogenesis and postnatal development but caused male infertility. This is consistent with the low expression of the mitochondrial isoform in most somatic tissues and its high abundance in spermatozoa [30,31]. Furthermore, mitochondrial GPx4 is essential for the development and survival of photoreceptors in vivo [32]. Mitochondria also expresses GPx1, present in various cell compartments and widely distributed in cellular tissues, which rapidly reduces  $\text{H}_2\text{O}_2$ , peroxynitrite and  $\text{fFA-OOHs}$ , but is unable to reduce complex  $\text{LFA-OOHs}$  [33]. The ability of some members of the Prx family to interact with phospholipid membranes and to reduce FA-OOHs was firstly demonstrated by Cha et al. in 2000 [34] who reported that human Prx2 rapidly reduces  $\text{fFA-OOH}$  and interacts with erythrocyte plasma membrane through a C-terminal region [34]. Mammalian Prx6 also reduces FA-OOHs forming part of phospholipids in membranes [35]. Some other Prxs reduce  $\text{fFA-OOHs}$  but have no- or only a very weak activity with  $\text{LFA-OOHs}$  [36–38]. In some cases,  $\text{fFA-OOHs}$  not only oxidize but also hyperoxidize Cys<sub>P</sub> [39,40]. The molecular basis for the oxidizing substrate specificity in Prxs is only starting to be unraveled [41]. Some previous data suggest that Prx3 might be able to catalyze the reduction of  $\text{fFA-OOHs}$ . For example, cells lacking Prx3 showed an increased susceptibility of the tumor suppressor protein PTEN, a member of the protein tyrosine phosphatase family, to be oxidized by a  $\text{fFA-OOH}$  [42]. Furthermore, Prx3 got hyperoxidized in cells exposed to AA-derived hydroperoxides [43]. However, since addition of  $\text{fFA-OOHs}$  to cells can lead to mitochondrial dysfunction and further oxidant production [44], a direct reaction of FA-OOHs and Prx3 remains to be investigated. Although the enzyme is mostly expressed in mitochondria, it can also be located in cell surfaces [45]. For instance, it was detected in membrane-enriched fractions from cancer cell lines exposed to RSL3, an inhibitor of GPx4 that causes ferroptosis. However, Prx3 siRNA failed to demonstrate a protective role against this form of death in those cells [46]. Interestingly, mouse embryonic fibroblast expressing a mutated form of GPx4 (Sec to Cys) showed a compensatory up-regulation of Prx3 [47]. Furthermore, overexpression of Prx3

ameliorates the symptoms of mild but not severe forms of ferroptosis of spinal motor neurons from GPx4 neuron inducible knockout mice [48].

Herein, we investigated the ability of human Prx3 (*HsPrx3*) to catalyze the reduction of FA-OOHs. In particular, we investigated the reactions of *HsPrx3* with  $\iota$ FA-OOHs involved in eicosanoid synthesis, i.e., derived from 15-lipoxygenase-catalyzed peroxidation of AA and EPA (15S-hydroperoxy-5Z,8Z,11Z,13E-eicosatetraenoic acid (15(S)-HpETE) and 15S-hydroperoxy-5Z,8Z,11Z,13E,17Z-eicosapentaenoic acid (15(S)-HpEPE), respectively) and derived from cyclooxygenase-catalyzed peroxidation of AA (the endoperoxide-hydroperoxide prostaglandin G<sub>2</sub> (PGG<sub>2</sub>)), which is a precursor for the 2-series prostaglandin and thromboxane synthesis (structures are shown in Supplementary Figure S1). Our data indicate that the enzyme is very rapidly oxidized as well as hyperoxidized by  $\iota$ FA-OOHs, alerts on the interpretation of kinetic results obtained by different methodologies and could help to explain at least in part Prx3 hyperoxidation detected in mammalian tissues [49,50].

## 2. Materials and Methods

### 2.1. Reagents

Dithiothreitol (DTT), N-ethylmaleimide (NEM), beta-mercaptoethanol ( $\beta$ -ME), reduced nicotinamide adenine dinucleotide phosphate (NADPH), isopropyl- $\beta$ -D-thiogalactopyranoside (IPTG), kanamycin sulphate, ampicillin, 2-iodoacetamide, diethylenetriaminepentaacetic acid (DTPA), 8-anilino-1-naphthalene sulfonic acid (ANS) and imidazol were from Sigma-Aldrich (Darmstadt, Germany). H<sub>2</sub>O<sub>2</sub> was obtained from Mallinckrodt Chemicals (St. Louis, MO, USA). 15(S)-HpETE ( $\geq 98\%$  pure), 15(S)-HpEPE ( $\geq 98\%$  pure), 9 $\alpha$ ,11 $\alpha$ -epidioxy-15S-hydroperoxy-prosta-5Z,13E-dien-1-oic acid (PGG<sub>2</sub>,  $\geq 95\%$  pure), arachidonic acid (AA,  $\geq 98\%$  pure) and eicosapentaenoic acid (EPA,  $\geq 98\%$  pure) (Supplementary Figure S1) were obtained from Cayman Chemical (Ann Arbor, MI, USA) as ethanolic solutions (or in acetone solution in the case of PGG<sub>2</sub>) and stored under argon at  $-80\text{ }^{\circ}\text{C}$ . All other reagents were obtained from standard commercial sources and used as received. Experiments were performed in 50 mM phosphate buffer plus 0.1 mM DTPA, pH 7.8 and  $25\text{ }^{\circ}\text{C}$ , except otherwise indicated.

### 2.2. Hydroperoxide Concentration Measurements

The concentration of H<sub>2</sub>O<sub>2</sub> was determined from absorbance measurements at 240 nm ( $\epsilon = 43.6\text{ M}^{-1}\text{cm}^{-1}$ ) [51].

Hydroperoxide consumption by *HsPrx3* under non-catalytic conditions was measured mixing reduced enzyme with the hydroperoxide of interest and determining remaining hydroperoxide concentrations after 30 s of incubation by the ferrous oxidation–xylenol orange method (FOX assay) [39,52]. The extinction coefficients for the different hydroperoxides using this assay were 15(S)-HpEPE,  $\text{Abs}_{560} = 60,000\text{ M}^{-1}\text{cm}^{-1}$ ; PGG<sub>2</sub>,  $\text{Abs}_{560} = 44,000\text{ M}^{-1}\text{cm}^{-1}$ ; H<sub>2</sub>O<sub>2</sub>,  $\text{Abs}_{560} = 43,000\text{ M}^{-1}\text{cm}^{-1}$ , which are in close agreement with previously reported values [39,53].

### 2.3. Enzyme Expression and Purification

Recombinant *HsPrx3* (wild type, wt*HsPrx3* as well as a Cys<sub>p</sub> to Ser mutated form, C<sub>p</sub>S*HsPrx3*) lacking the mitochondrial targeting sequence and containing three additional N-terminal Gly residues were expressed in BL21 Star (DE3) *Escherichia coli* strain and purified as previously reported [13]. Human thioredoxin 1 (*HsTrx1*), which acts as an efficient reducing substrate for *HsPrx3* in vitro [54], was expressed as in [55]. The plasmid for recombinant expression of *Echinococcus granulosus* thioredoxin glutathione reductase lacking the glutaredoxin (Grx) domain (*EgTR*) was obtained from Mariana Bonilla and Lucía Turell, from Institut Pasteur Montevideo and Universidad de la República, Montevideo, Uruguay, respectively, and was expressed and purified as previously [56].

Protein concentrations were measured at 280 nm using extinction coefficients of  $19,940\text{ M}^{-1}\text{cm}^{-1}$  per reduced *HsPrx3* subunit and  $7100\text{ M}^{-1}\text{cm}^{-1}$  for *HsTrx1* as previously [13]. *EgTR* protein concentration was measured as in [56].

#### 2.4. Reduction of HsPrx3

In some experiments, HsPrx3 was reduced immediately before use by incubating the enzyme with DTT (2 mM) for 30 min on ice. Excess reductant was removed by gel filtration using a HiTrap desalting column (Amersham Biosciences, Amersham, UK) and freshly made degassed sodium phosphate buffer 50 mM plus 0.1 mM DTPA, pH 7.8.

#### 2.5. Catalytic Activity of HsPrx3

The catalytic activities of HsPrx3 using H<sub>2</sub>O<sub>2</sub> or different *f*FA-OOHs as oxidizing substrates were measured using a coupled assay following NADPH oxidation at 340 nm ( $\epsilon_{340\text{ nm}} = 6220\text{ M}^{-1}\text{s}^{-1}$ ) (150  $\mu\text{M}$ ) [57] in the presence of EgTR (40 nM), HsTrx1 (30  $\mu\text{M}$ ) and HsPrx3 (0.8  $\mu\text{M}$ ) in sodium phosphate buffer 50 mM plus 0.1 mM DTPA at pH 7.8 and 25 °C. The mixture was pre-incubated during a minute and the reaction was started by adding 20  $\mu\text{M}$  of the indicated hydroperoxide, rapidly mixed in a vortex and transferred to a cuvette to start measurements. In order to determine whether the enzyme remained active after the incubation with the hydroperoxide of interest, H<sub>2</sub>O<sub>2</sub> (20  $\mu\text{M}$ ) was added 3 min after the initial incubation. Control experiments using different concentrations of EgTR and HsPrx3 were performed to ensure that reduction of HsTrx1 by EgTR was not rate limiting the oxidation of NADPH by the hydroperoxides of interest in the presence of EgTR, HsTrx1 and HsPrx3. EgTR, which as mammalian TR is a selenium-containing protein, was used due to its availability as a highly pure recombinant protein in our lab. Measurements were performed using a Shimadzu UV-Vis spectrophotometer (Shimadzu, Kyoto, Japan) equipped with a Peltier-based temperature control.

#### 2.6. Kinetics of HsPrx3 Oxidation and Hyperoxidation by *f*FA-OOHs

As in other members of the typical two-cysteine Prx family [58–60], changes in the redox state of Cys<sub>P</sub> of HsPrx3 are accompanied by changes in the tryptophan-dependent intrinsic fluorescence intensity of the protein [13]. The oxidation of the thiol group in HsPrx3 Cys<sub>P</sub> to sulfenic acid causes a rapid decrease in intrinsic fluorescence while resolution causes a slower phase of fluorescence increase. Since oxidation is a bimolecular process, the observed rate constant of the decrease in intrinsic fluorescence depends on the concentration of the oxidant. On the contrary, resolution is an intramolecular process and its rate constant is independent on the oxidant concentration. Hyperoxidation can compete with resolution leading to an acceleration of the second phase of fluorescence change (Supplementary Figure S2). We therefore took advantage of this fluorescence behavior of the protein to measure the kinetics of HsPrx3 Cys<sub>P</sub> oxidation and hyperoxidation. Reduced wt or C<sub>P</sub>SHsPrx3 in 50 mM sodium phosphate buffer plus 0.1 mM DTPA pH 7.8 in one syringe was rapidly mixed with the indicated concentrations of the hydroperoxide of interest in the same buffer from a second syringe at 11–12 °C, and the protein intrinsic fluorescence changes were recorded using a SX20 Applied Photophysics stopped-flow spectrofluorimeter (Applied Photophysics, Leatherhead, UK) ( $\lambda_{\text{ex}} = 295\text{ nm}$ , total emission). Data were fitted by exponential functions to obtain the observed rate constants of each phase ( $k_{\text{obs}}$ ). The rate constants of the reaction of HsPrx3 Cys<sub>P</sub> oxidation and hyperoxidation were calculated from the slope of the plot of the  $k_{\text{obs}}$  of the decrease phase and the increase phase of fluorescence change, respectively, plotted versus hydroperoxide concentration.

#### 2.7. SDS PAGE and Western Blot Analysis of HsPrx3 Hyperoxidation

Reduced HsPrx3 (5  $\mu\text{M}$ ) was treated with the indicated concentrations of H<sub>2</sub>O<sub>2</sub> or *f*FA-OOHs in sodium phosphate buffer 50 mM pH 7.8 plus 0.1 mM DTPA. After 15 min, the alkylating agent NEM (20 mM) was added. Samples were resolved in 15% SDS-PAGE electrophoresis under non-reducing (− $\beta$ -ME) or reducing (+ $\beta$ -ME) conditions and were stained using Coomassie. Alternatively, samples were transferred to a nitrocellulose membrane to detect HsPrx3 Cys<sub>P</sub> hyperoxidation to sulfinic/sulfonic (Cys<sub>P</sub>-SO<sub>2/3</sub>H) acid using a commercial rabbit polyclonal antiPrx-Cys<sub>P</sub>-SO<sub>2/3</sub>H antibody (Abcam, 1b16830,

Waltham, MA, USA). Secondary anti-rabbit antibodies were IR-Dye 800CW and data were acquired using an Odyssey imaging system from LI-COR Bioscience (Lincoln, NE, USA).

### 2.8. Mass Spectrometry Analysis of HsPrx3 Modifications by FA-OOHs

Reduced HsPrx3 (10  $\mu\text{M}$ ) in 50 mM phosphate buffer plus 0.1 mM DTPA (pH 7.8, 25  $^{\circ}\text{C}$ ) without further treatment, exposed to 15(S)-HpEPE (10 or 20  $\mu\text{M}$ ) or to  $\text{H}_2\text{O}_2$  (20  $\mu\text{M}$ ) were alkylated with 2-iodoacetamide (5 mM) for 30 min at 37  $^{\circ}\text{C}$ . The excess alkylating agent was removed by gel filtration using PD SpinTrap G-25 columns (GE Healthcare, Chicago, IL, USA) equilibrated with 20 mM ammonium bicarbonate buffer (pH 7.4, 25  $^{\circ}\text{C}$ ). All samples were loaded into a C4 column (214MS5115, Grace Vydac, Hesperia, CA, USA) for HPLC separation. Mobile phase consisted of 0.1% formic acid in nanopure water (solvent A) and 0.1% formic acid in  $\text{CH}_3\text{CN}$  (solvent B), and elution of the protein was performed with a 10-min linear gradient of solvent B (5–50%) followed by an additional 10 min at 50% solvent B at 100  $\mu\text{L}/\text{min}$ . An ESI-triple quadrupole mass spectrometer (QTRAP4500, ABSciex Framingham, MA, USA) was employed for detection. The spectrometer was set in Q1 positive mode in the 500–2000  $m/z$  range with a scan rate of 200 Da/s and Q1 resolution in unit. Parameters used were as follows: Ion Sray voltage, 5000 V; Ion Source Temperature, 300  $^{\circ}\text{C}$ ; Declustering Potential, 120 V; Entrance Potential, 10; Curtain Gas, 20 psi; Gas1, 30 psi; Gas2, 20 psi. Data acquisition was performed using Analyst 1.6.2 (ABSciex) and PeakView 2.2 (ABSciex) software was used for data analysis and deconvolution of all spectra.

### 2.9. Fatty Acids Binding to HsPrx3

The ability of HsPrx3 to bind fatty acids (FAs) was evaluated by two different experimental methodologies. Firstly, we analyzed the interactions of HsPrx3 with ANS, a fluorescent compound used as a probe of protein surface hydrophobicity in the proximity of cationic groups [61,62]. ANS binding to this protein microenvironment leads to a blue shift and an increase in the probe quantum yield. Furthermore, due to its spectral properties ANS could lead to intrinsic, tryptophan-dependent protein fluorescence resonance energy transfer (FRET) [63]. Fluorescence measurements were performed using a Jasco FP-8500 spectrofluorimeter and 500  $\mu\text{L}$ , 10 mm path length quartz cuvettes. For direct fluorescence measurements, excitation was performed at 375 nm and emission spectra (440–600 nm) were obtained. HsPrx3 (5  $\mu\text{M}$ ) was titrated with ANS in sodium phosphate buffer 50 mM pH 7.8 plus 0.1 mM DTPA. Control experiments in the absence of HsPrx3 were also performed. In FRET experiments, HsPrx3 (2  $\mu\text{M}$ , 5  $\mu\text{M}$  and 8  $\mu\text{M}$ ) was excited at 295 nm, and emission spectra were recorded between 315 nm and 550 nm. Binding constants were obtained fitting the plot of change in intrinsic fluorescence intensity versus ANS concentration to hyperbolic functions as well as through Scatchard analysis.

Additionally, heat unfolding experiments of HsPrx3 in the absence and presence of AA were performed to analyze the effect of the FA on the thermal stability of the protein. Briefly, the tryptophan-dependent intrinsic fluorescence intensity of HsPrx3 (4  $\mu\text{M}$ ) ( $\lambda_{\text{ex}} = 295 \text{ nm}$ ,  $\lambda_{\text{em}} = 335 \text{ nm}$ ) in the absence or presence of AA (10 or 20  $\mu\text{M}$ ) plus an excess of DTT (2 mM) was registered in a Jasco FP-8500 spectrofluorimeter (Jasco, Tokyo, Japan), while an increase in temperature (35–70  $^{\circ}\text{C}$ ) with a heating rate of 1.5  $^{\circ}\text{C}/\text{min}$  was applied to the sample. Sample buffer was 50 mM phosphate buffer plus 0.1 mM DTPA, pH 7.8 and a 10 mm path length quartz cuvette (500  $\mu\text{L}$ ) was used. The apparent melting temperatures ( $T_m$ ) as midpoint of the denaturation curves were obtained fitting the data to a sigmoidal function.

### 2.10. Computer-Assisted Molecular Modeling of FA Binding to HsPrx3

To perform docking simulations of the binding of 15(S)-HpETE to reduced HsPrx3, a dimeric unit made of chains A and B was extracted from its reported crystal structure PDB id 5jcg and subjected to a short molecular dynamic [64] simulation [64] as previously reported by our group [40,41]. Briefly, the dimer was solvated using a default method,

with an octahedral box of 12 Å in radius with TIP3P water molecules [65]. Protein residue parameters correspond to the parm14SB Amber force field [66]. MD was performed using periodic boundary conditions with a 10 Å cutoff and particle mesh Ewald (PME) summation method for treating the electrostatic interactions. The hydrogen bond lengths were kept at their equilibrium distance by using the SHAKE algorithm, while temperature and pressure were kept constant with a Langevin thermostat and barostat, respectively, as implemented in the AMBER program (Amber, University of California, San Diego, CA, USA) [67]. The system was optimized in 1000 steps (10 with steep gradient and the rest with conjugate gradient). Then, it was slowly heated from 0 K to 300 K for 20 ps at constant pressure, with Berendsen thermostat, and pressure was equilibrated at 1 bar for 5 ps. After these two steps, a 10 ns long MD simulation at constant temperature (300 K) and constant volume was performed, followed by a 200 ns long trajectory. The last structure resulting from the MD was used for the molecular docking of 15(S)-HpETE. The structure of the enzyme was considered rigid while 15(S)-HpETE was allowed to be flexible. 500 binding modes were generated and analyzed using standard protocols of AutoDock4.2.6 (The Scripps Research Institute, La Jolla, CA, USA) [68].

### 2.11. Simulations of HsPrx3 Hyperoxidation by Fluxes of Mitochondrial Hydroperoxides in the Presence of Peroxidases

Simulations were performed using COPASI 4.37 program. Rate constants, reactant concentrations and formation rates of H<sub>2</sub>O<sub>2</sub> and  $\gamma$ FAOOH are indicated in the text.

## 3. Results

### 3.1. HsPrx3 Is Rapidly Inactivated by $\gamma$ FA-OOHs

HsPrx3 catalyzed the reduction of H<sub>2</sub>O<sub>2</sub> (20  $\mu$ M) as detected by a decrease in NADPH concentration in the coupled assay described in Methods. No consumption of NADPH was observed in the absence of HsPrx3 (not shown). The reaction ended due to oxidizing substrate depletion and not because of enzyme inactivation due to hyperoxidation, since a new addition of H<sub>2</sub>O<sub>2</sub> to the cuvette caused a new phase of NADPH consumption of similar rate. This is consistent with previous data indicating that the rate constant of HsPrx3 hyperoxidation by H<sub>2</sub>O<sub>2</sub> is  $1.1 \times 10^3 \text{ M}^{-1}\text{s}^{-1}$  versus a rate constant of resolution of  $2 \text{ s}^{-1}$  at pH 7.8 and 25 °C [13], which indicates that at 20  $\mu$ M H<sub>2</sub>O<sub>2</sub> only ~1% of the enzyme would be hyperoxidized in the first catalytic cycle, a percentage/cycle that should decrease as the oxidant gets consumed. On the contrary, very slow rates of NADPH consumptions were observed when 15(S)-HpETE or 15(S)-HpEPE were used as substrates in the coupled assay. The addition of H<sub>2</sub>O<sub>2</sub> (20  $\mu$ M) to the cuvette at the end of the reaction failed to cause a decrease in NADPH concentration, indicating that HsPrx3 was inactive (Figure 1). The rate of NADPH consumption was modest in the case of PGG<sub>2</sub> (Table 1).

**Table 1.** Catalytic activity of HsPrx3 using different oxidizing substrates.

Oxidizing Substrate	$v_o$ <sup>1</sup> ( $\mu$ M/s)	$v_o$ after Subsequent Addition of 20 $\mu$ M H <sub>2</sub> O <sub>2</sub> ( $\mu$ M/s)
H <sub>2</sub> O <sub>2</sub>	0.55	0.60
15(S)-HpETE	0.07	0.03
15(S)-HpEPE	0.08	0.02
PGG <sub>2</sub>	0.09	0.08

<sup>1</sup> Initial rate here means the rate at the beginning of data acquisition, 15 s after the addition of the oxidizing substrate.

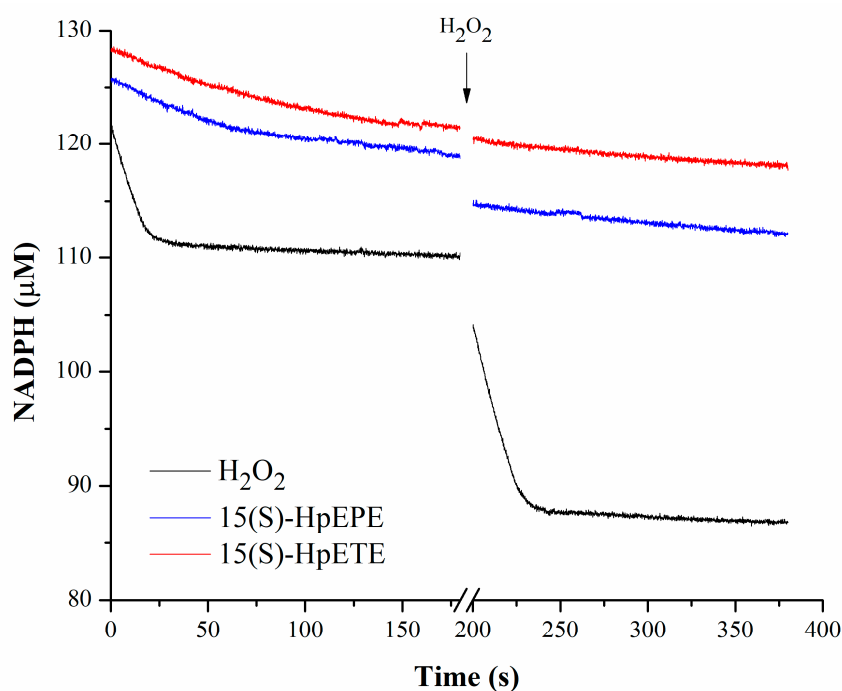


**Figure 1.** Inactivation of *HsPrx3* by  $\iota$ FA-OOHs. NADPH was pre-incubated with *EgTR* (40 nM), *HsTrx1* (30  $\mu$ M) and *HsPrx3* (0.8  $\mu$ M) and rapidly mixed with the indicated oxidizing substrates (20  $\mu$ M) (black,  $H_2O_2$ ; blue, 15(S)-HpEPE; red, 15(S)-HpETE) in sodium phosphate buffer 50 mM plus 0.1 mM DTPA, pH 7.8 and 25  $^{\circ}$ C. The arrow indicates the addition of  $H_2O_2$  (20  $\mu$ M) to the mixture.

### 3.2. Kinetics of *HsPrx3* Oxidation by $\iota$ FA-OOH

The addition of 15(S)-HpETE (Figure 2A), 15(S)-HpEPE (Figure 2B), and PGG<sub>2</sub> (Figure 2C) in excess to reduced *HsPrx3* caused a very rapid decrease in the enzyme intrinsic fluorescence (phase of oxidation of the thiolate in Cys<sub>P</sub> to sulfenic acid), followed by a slower phase of fluorescence increase (resolution plus hyperoxidation phase) (Supplementary Figure S2). In the case of 15(S)-HpETE and 15(S)-HpEPE, the first phase was so rapid that it was complete in a few ms even at the lower concentrations of oxidant tested (Figure 2A,B). A half-life of oxidation reaction of <10 ms for  $\iota$ FA-OOHs concentrations of 1.5–2  $\mu$ M as obtained for both 15(S)-HpETE and 15(S)-HpEPE is consistent with rate constants of  $>3.5 \times 10^7 \text{ M}^{-1}\text{s}^{-1}$  at pH 7.8 and 12  $^{\circ}$ C. In the case of PGG<sub>2</sub>, the oxidation phases were slower and fitted to exponentials. From the plot of  $k_{obs}$  of the first phase versus the concentration of PGG<sub>2</sub>, the rate constant of *HsPrx3* oxidation by this  $\iota$ FA-OOH was obtained as  $(2.4 \pm 0.4) \times 10^7 \text{ M}^{-1}\text{s}^{-1}$  (Figure 2C inset). From the slopes of the plots of  $k_{obs}$  of the second phase of fluorescence change versus the concentration of 15(S)-HpETE, 15(S)-HpEPE and PGG<sub>2</sub> the rate constants of hyperoxidation were obtained as  $(1.7 \pm 0.1) \times 10^7$ ,  $(2.6 \pm 0.4) \times 10^7$  and  $(3.1 \pm 0.7) \times 10^5 \text{ M}^{-1}\text{s}^{-1}$ , respectively, (Figure 2D). As controls, the addition of the non-peroxidized fatty acid EPA (3  $\mu$ M) to reduced *HsPrx3* (0.3  $\mu$ M) caused no change in the protein intrinsic fluorescence. Similarly, the addition of PGG<sub>2</sub> to reduced C<sub>P</sub>SHsPrx3 (0.3  $\mu$ M) caused no change in protein intrinsic fluorescence, consistent with the requirement of both Cys<sub>P</sub> in *HsPrx3* and the hydroperoxide group in the fatty acid for the reaction to occur (Figure 2E,F).

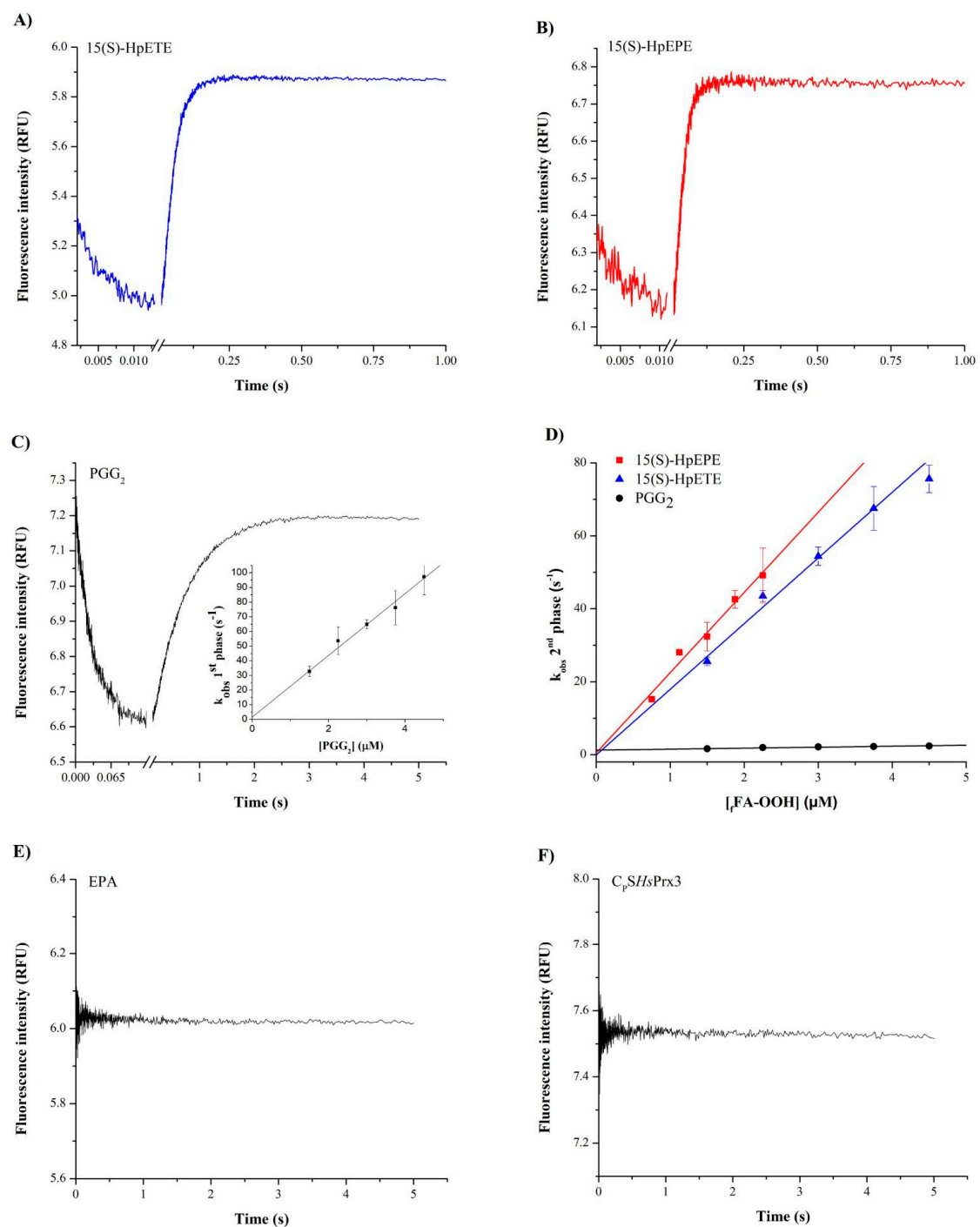


**Figure 2.** Kinetics of *HsPrx3* oxidation and hyperoxidation by  $f$ FA-OOHs. Reduced *HsPrx3* (0.3 μM final concentration) was rapidly mixed with 15(S)-HpETE (A), 15(S)-HpEPE (B) and PGG<sub>2</sub> (C) (1.5 μM final concentration) in sodium phosphate buffer 50 mM plus 0.1 mM DTPA at pH 7.8 and 12 °C. The time courses of intrinsic fluorescence intensity change were followed ( $\lambda_{ex} = 295$  nm, total emission). The inset of (C) shows a linear fit of  $k_{obs}$  of fluorescence intensity decay plotted versus PGG<sub>2</sub> concentration from which the second order rate constant of *HsPrx3* oxidation by PGG<sub>2</sub> was obtained. The rate constant of hyperoxidation of Cys<sub>p</sub> was determined for the three  $f$ FA-OOHs mentioned above, plotting the  $k_{obs}$  of the phases of fluorescence intensity recovery against  $f$ FA-OOH concentration (D). Both in inset of (C) and in (D) the symbols and error bars represent medians and standard deviations from at least 5 replicates of one of the three independent experiments performed. The effect of EPA (3 μM) on the intrinsic fluorescence of reduced *HsPrx3* (0.3 μM) (E) and of PGG<sub>2</sub> (0.3 μM) on C<sub>p</sub>SHsPrx3 (0.3 μM) (F) are also shown.

### 3.3. Consumption of Hydroperoxides by HsPrx3 under Non-Catalytic Conditions

When  $\text{H}_2\text{O}_2$  (50  $\mu\text{M}$ ) was mixed with reduced HsPrx3 (20  $\mu\text{M}$ ) a fast consumption of 0.8 equivalents of hydroperoxide by HsPrx3 occurred. Similarly, a 1:1 consumption of  $\text{PGG}_2$ /HsPrx3 was obtained. However, the stoichiometry of hydroperoxide consumption was higher (1.7:1) for 15(S)-HpEPE. This is consistent with a fast hyperoxidation process in the case of 15(S)-HpEPE that consumes a second equivalent of oxidant (Figure 3).

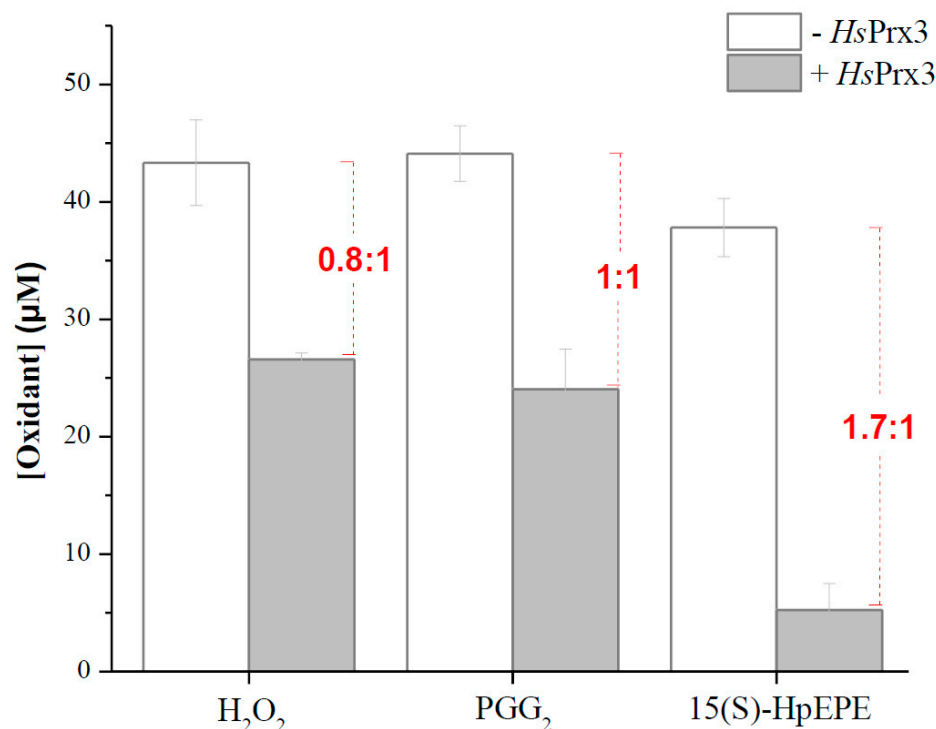


**Figure 3.** Stoichiometry of hydroperoxide consumption by HsPrx3. 15(S)-HpEPE and  $\text{PGG}_2$  consumption by HsPrx3.  $\text{H}_2\text{O}_2$ ,  $\text{PGG}_2$  and 15(S)-HpEPE (left to right) decay in sodium phosphate buffer 50 mM (pH 7.8, 25 °C) in the absence (white bars) or 30 s after the addition of 20  $\mu\text{M}$  reduced HsPrx3 (grey bars). Numbers in red represent the stoichiometry of hydroperoxide consumption.

### 3.4. HsPrx3 Is Hyperoxidized at Low Concentrations of $\beta$ FA-OOHs

#### 3.4.1. SDS PAGE and Western Blot Analysis

Reduced HsPrx3 (5  $\mu\text{M}$ ) without any further addition in the absence of  $\beta$ -ME (Supplementary Figure S3, lane 1) was mostly monomeric although it contained a minor proportion of oxidized to disulfide dimeric enzyme that reverted to the monomeric form in the presence of  $\beta$ -ME (Supplementary Figure S3, lane 2), consistent with the 0.8  $\text{H}_2\text{O}_2$ /HsPrx3 stoichiometry of hydroperoxide consumption shown in Figure 3. The addition of  $\text{H}_2\text{O}_2$  (500  $\mu\text{M}$ , lanes 3 and 4) or 15(S)-HpETE (10  $\mu\text{M}$ , lanes 5 and 6) to reduced HsPrx3 (5  $\mu\text{M}$ ) caused an increase in the dimeric form of the enzyme in the samples without  $\beta$ -ME (lanes 3 and 5) that were fully reverted to the monomeric form in the presence of the reductant (lanes 4 and 6). The presence of monomeric form of the enzymes in samples treated with excess hydroperoxides and without  $\beta$ -ME are consistent with the formation of hyperoxidized monomers as confirmed by Western Blot (see below).

When reduced HsPrx3 (5  $\mu\text{M}$ ) was exposed to  $\text{H}_2\text{O}_2$ , hyperoxidation of  $\text{Cys}_\text{P}$  was only marginally detected unless excess oxidant was used. As reported [14], hyperoxidation by  $\text{H}_2\text{O}_2$  occurred firstly in one of the subunits of the dimer, while the other was forming an inter-subunit disulfide which is detected as a hyperoxidized dimer, and only at concentrations of  $\text{H}_2\text{O}_2 \geq 500 \mu\text{M}$  hyperoxidized monomers, i.e., subunits with both  $\text{Cys}_\text{P}$  hyperoxidized, were detected (Figure 4A). On the contrary, both 15(S)-HpETE and 15(S)-HpEPE caused HsPrx3  $\text{Cys}_\text{P}$  hyperoxidation at lower concentrations, even equimolar,

that was detected in both the monomeric and dimeric forms of the protein, in agreement with a fast kinetics of hyperoxidation. PGG<sub>2</sub>-mediated hyperoxidation profile was similar to that of H<sub>2</sub>O<sub>2</sub>, leading to hyperoxidized dimers at concentrations  $\leq 50$   $\mu$ M (not shown).

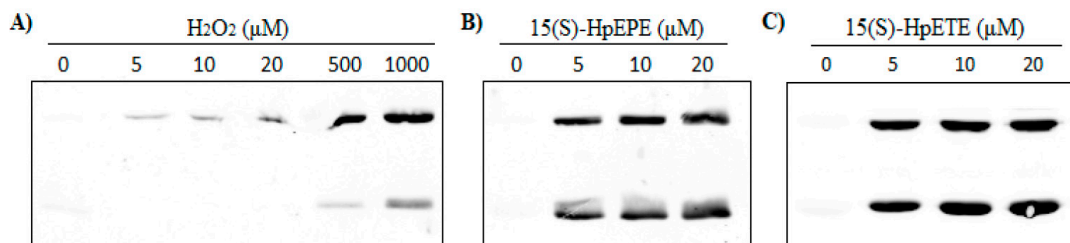


**Figure 4.** Hyperoxidation of *HsPrx3* by different hydroperoxides. Reduced *HsPrx3* (5  $\mu$ M) was treated with the indicated concentrations of (A) H<sub>2</sub>O<sub>2</sub>; (B) 15(S)-HpEPE; and (C) 15(S)-HpETE in sodium phosphate buffer 50 mM pH 7.8 plus 0.1 mM DTPA. The samples were alkylated and used for Western Blot detection of Cys<sub>P</sub> hyperoxidation.

### 3.4.2. Mass Spectrometry Analysis

In order to confirm the hyperoxidation of *HsPrx3* treated with *t*-FA-OOHs, MS analysis was performed. The predicted molecular weight of the reduced *HsPrx3* subunit is 21,797 Da (13). Treatment with excess 2-iodoacetamide caused alkylation of reduced *HsPrx3* (major peaks of +113 and +170 which corresponds to the covalent addition of 2 and 3 carbamidomethyl (CAM) groups (+57 each), respectively, Figure 5A and Table 2). The presence of a small fraction of a form of the protein modified by 4 CAM groups in the reduced enzyme that has three Cys residues in its sequence is consistent with the reported side reaction of the alkylating agent with N-terminal as well as side chain amine groups [69]. When reduced *HsPrx3* was exposed to H<sub>2</sub>O<sub>2</sub> (1:2 concentration ratio) and then alkylated, the main products detected were the dimeric oxidized disulfide form of the enzyme as well as alkylated derivatives (Figure 5B and Table 2). However, when reduced *HsPrx3* was treated with a 1:1 concentration ratio of 15(S)-HpEPE and then treated with iodoacetamide, the main products had an increase in mass of +89, consistent with CAM addition (+57) plus hyperoxidation (+32) (Figure 5C and Table 2). When the concentration of 15(S)-HpEPE was further increased (2:1 concentration ratio) the major species detected had a mass increment of +104, consistent with CAM addition plus the addition of 3 oxygen atoms (Figure 5C and Table 2). This +104 modification was observed in the monomeric and also in the dimeric form of the enzyme exposed to 15(S)-HpEPE (Table 2). The latter is ascribed to Cys<sub>P</sub> hyperoxidation to sulfonic acid (+48), since similar addition of 2:1 concentration of 15(S)-HpEPE to C<sub>P</sub>SHsPrx3 yielded a +57 form, consistent with alkylation of the enzyme as the major product (Figure 5D and Table 2).

### 3.5. Biophysical Experiments Suggest the Binding of Hydrophobic Compounds to *HsPrx3*

#### 3.5.1. Binding of ANS and AA to *HsPrx3*

The addition of increasing concentrations of ANS to *HsPrx3* (5  $\mu$ M) in sodium phosphate buffer 50 mM, pH 7.8 plus 0.1 mM DTPA, showed an increase in ANS quantum yield ( $\lambda_{\text{ex}} = 375$  nm) and a blue shift when compared with equal concentrations of ANS in the same buffer in the absence of the enzyme (Figure 6A). Additionally, ANS caused a decrease in tryptophan-dependent *HsPrx3* fluorescence emission at 339 nm ( $\lambda_{\text{ex}} = 295$  nm) (Figure 6A) consistent with FRET, as previously reported for several proteins that bind ANS, including the peroxiredoxin AhpE from *Mycobacterium tuberculosis* [41]. Relative intrinsic fluorescence change ( $1 - F/F_0$ ) exhibited a hyperbolic behavior when plotted against ANS concentration, resulting in saturation curves from which the value of the dissociation constant ( $K_d$ ) of  $65 \pm 4$   $\mu$ M and number of binding sites ( $n$ ) of  $1.34 \pm 0.05$  were obtained. The inset in Figure 6B shows a Scatchard linealization of the data obtained at 2  $\mu$ M *HsPrx3*, which yielded similar parameters. The addition of the saturated fatty

acid palmitic acid at concentrations below its CMC (60  $\mu\text{M}$ ) [70] did not compete with the binding of ANS to the enzyme (not shown).

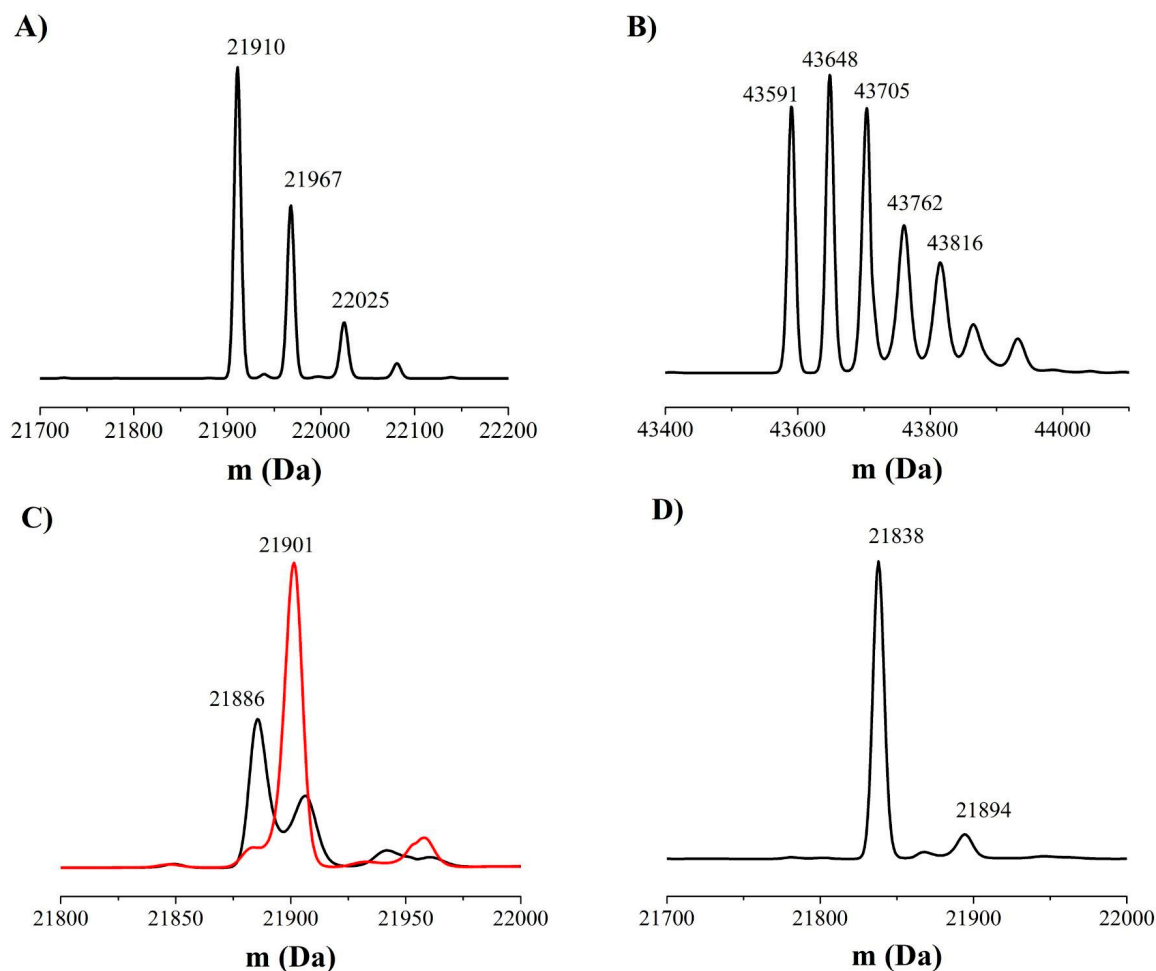


**Figure 5.** MS analysis of the modifications of *HsPrx3* caused by 15(S)-HpEPE. Mass spectrum of (A) reduced *HsPrx3* (10  $\mu\text{M}$ ); (B) reduced *HsPrx3* treated with  $\text{H}_2\text{O}_2$  (20  $\mu\text{M}$ ); (C) reduced *HsPrx3* treated with 15(S)-HpEPE (10  $\mu\text{M}$ , black trace; and 20  $\mu\text{M}$ , red trace); and (D) reduced  $\text{C}_\text{p}\text{SHsPrx3}$  treated with 15(S)-HpEPE (20  $\mu\text{M}$ ). All samples were alkylated with excess 2-iodoacetamide after treatment (5 mM).

**Table 2.** Mass spectrometry analysis of *HsPrx3* modifications caused by  $\text{H}_2\text{O}_2$  and 15(S)-HpEPE.

Treatment	Mass (Da)	Peak Description
Reduced <i>HsPrx3</i>	21,910	<i>HsPrx3</i> -2CAM
	21,967	<i>HsPrx3</i> -3CAM
	22,025	<i>HsPrx3</i> -4CAM
<i>HsPrx3</i> + $\text{H}_2\text{O}_2$	43,591	<i>HsPrx3</i> dimer
	43,648	<i>HsPrx3</i> -CAM dimer
	43,705	<i>HsPrx3</i> -2CAM dimer
	43,762	<i>HsPrx3</i> -3CAM dimer
	43,816	<i>HsPrx3</i> -4CAM dimer
<i>HsPrx3</i> + 15(S)-HpEPE	21,886	CAM- <i>HsPrx3</i> - $\text{SO}_2$
	43,696	CAM- <i>HsPrx3</i> - $\text{SO}_3$ dimer
	21,901	CAM- <i>HsPrx3</i> - $\text{SO}_3$
$\text{C}_\text{p}\text{SHsPrx3}^* + 15(\text{S})\text{-HpEPE}$	21,838	$\text{C}_\text{p}\text{SHsPrx3}$ -CAM
	21,894	$\text{C}_\text{p}\text{SHsPrx3}$ -2CAM

\* the predicted molecular weight of wild type and  $\text{C}_\text{p}\text{SHsPrx3}$  reduced subunit are 21,797 Da [13] and 21,781 Da, respectively.

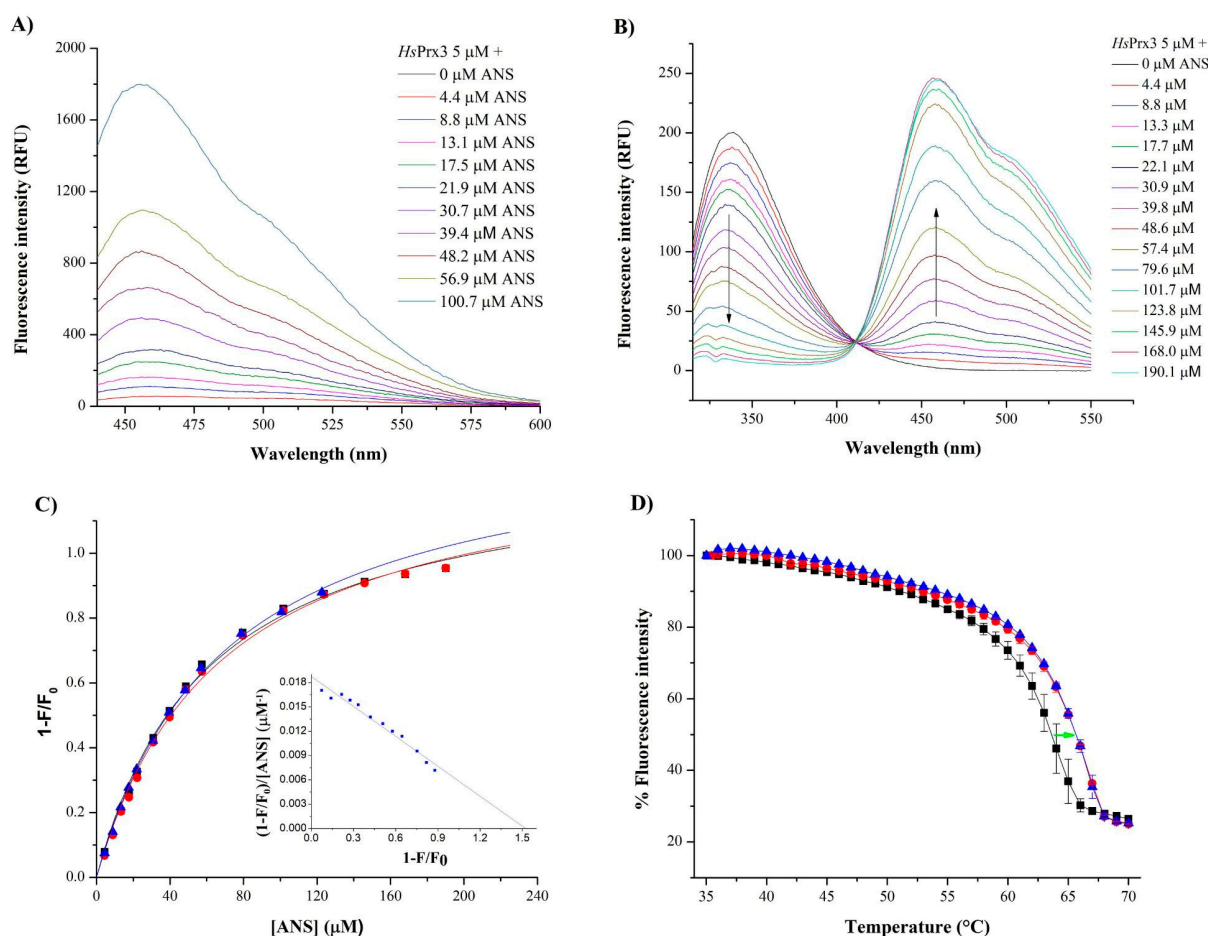


**Figure 6.** Binding of ANS and AA to HsPrx3. (A) Direct fluorescence measurement of ANS at an excitation wavelength of 375 nm. For each ANS concentration, the spectrum shown corresponds to the difference between the recorded spectra in the presence and in the absence of HsPrx3 (5 μM). (B) HsPrx3 (5 μM) was incubated with increasing ANS concentrations and fluorescence emission spectra ( $\lambda_{ex} = 295$  nm) were registered. The arrows indicate the direction of fluorescence changes observed after addition of different concentrations of ANS. (C) For three different protein concentrations (2 (▲), 5 (●) and 8 (■) μM), relative intrinsic fluorescence changes were plotted against [ANS], resulting in saturation curves which were fitted to hyperbolic functions. An example of the linearization through Scatchard plot corresponding to 2 μM HsPrx3 is shown in the inset. (D) Heat unfolding transitions following the intrinsic fluorescence intensity ( $\lambda_{ex} = 295$  nm,  $\lambda_{em} = 335$  nm) of the tryptophans of HsPrx3 (4 μM) in the absence (■) and presence of AA (10 μM (●) and 20 μM (▲)) and DTT (2 mM). Green arrow shows the shift in the apparent  $T_m$  in the presence of AA.

The apparent melting temperature ( $T_m$ ) of reduced HsPrx3 (4 μM) increased in the presence of AA (10 μM) and did not further increase in the presence of higher AA concentrations (20 μM), with  $T_m$  values of  $64.6 \pm 1$  °C for HsPrx3,  $68.1 \pm 1$  °C for HsPrx3 + AA (10 μM) and  $67.2 \pm 0.3$  °C for HsPrx3 + AA (20 μM) (AA critical micelle concentration ranges between 10–60 μM [71,72]). Addition of similar concentrations of FA solvent (ethanol) caused no change in protein  $T_m$  value (Supplementary Figure S4). This ~4 °C shift is consistent with the ability of HsPrx3 to interact with AA [73].

### 3.5.2. Modeling 15(S)-HpETE Binding to HsPrx3

The HsPrx3 dimeric unit arising from MD simulations using PDBid 5jcg chains A and B as starting point presents a hydrophobic patch close to Cys<sub>P</sub> with a solvent accessible surface area value of  $256 \pm 26$  Å<sup>2</sup> (Figure 7A). This region presents hydrophobic residues from both chains of the dimer, namely: Y39, P40, F43, F45, L142, P143, V167' and P181'. The

lowest energy binding modes of 15(S)-HpETE obtained by molecular docking simulations use this hydrophobic region for binding as shown in Figure 7B. Among these conformations, the most populated best ranked cluster presents the hydroperoxide group of 15(S)-HpETE in proximity to the thiolate of Cys<sub>P</sub> (Figure 7C). Those were also the structures of overall lower energy, indicating that the hydroperoxide group of the  $\gamma$ FA-OOH may also contribute to substrate pose.

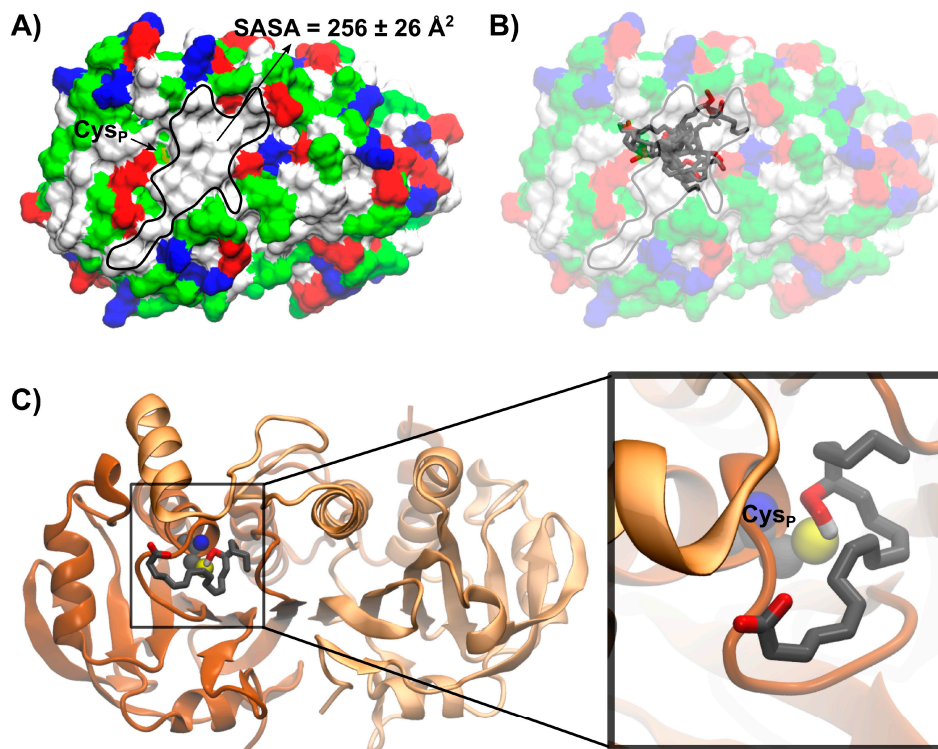


**Figure 7.** Best ranked structures of the binding of 15(S)-HpETE to *HsPrx3* obtained by docking simulations. (A) Surface representation of *HsPrx3* dimer colored by amino acid properties: white, hydrophobic; green, polar; blue, basic; red, acidic. The hydrophobic patch close to Cys<sub>P</sub> is highlighted and the solvent accessible surface area (SASA) value measured during the MD simulation is shown. (B) Superimposed 15(S)-HpETE representative structures of the ten best ranked clusters with at least five structures obtained by molecular docking. Hydrogen atoms are not shown for simplicity. (C) Representative structure of the most populated best ranked cluster from the molecular docking of 15(S)-HpETE to the *HsPrx3* dimer structure. Only the hydroperoxide hydrogen atom is shown for simplicity.

#### 4. Discussion

*HsPrx3* was almost inactive in catalyzing the reduction of 20  $\mu$ M 15(S)-HpETE and 15(S)-HpEPE by *HsTrx1* after 15 s required for appropriate mixing for measurements in a conventional spectrophotometer. Moreover, the enzyme lost its activity towards H<sub>2</sub>O<sub>2</sub> after being treated with those  $\gamma$ FA-OOHs (Figure 1 and Table 1). However, the enzyme consumed 1.7 15(S)-HpEPE per reduced *HsPrx3* under non-catalytic conditions (Figure 3), indicating that the lack of enzymatic activity shown in Figure 1 could be due to a rapid inactivation caused by hyperoxidation of Cys<sub>P</sub>. In the case of H<sub>2</sub>O<sub>2</sub>, in which hyperoxidation should not compete with resolution at low oxidant concentrations (see below) the stoichiometry was 0.8 hydroperoxide consumed per *HsPrx3*. Furthermore, one PGG<sub>2</sub> was consumed per *HsPrx3* (Figure 3), in agreement with its lower inactivation by this oxidant under catalytic conditions (Table 1) compared with 15(S)-HpEPE. The fact that reduced *HsPrx3* consumed less than one H<sub>2</sub>O<sub>2</sub> per protein reflects a minor fraction of oxidized enzyme (~20%) in

our sample after reduction and excess DTT removal (Supplementary Figure S3) due to the presence of adventitious  $H_2O_2$  in buffer solutions as already reported [74].

The addition of equimolar or higher concentrations of 15(S)-HpETE or 15(S)-HpEPE to HsPrx3 caused hyperoxidation of Cys<sub>P</sub> as detected by Western Blot analysis (Figure 4). In consonance, MS confirmed hyperoxidation to Cys<sub>P</sub> sulfinic acid even when added at equimolar concentration with respect to the enzyme. Additionally, in the presence of excess 15(S)-HpEPE, HsPrx3 Cys<sub>P</sub> was not only oxidized to sulfinic acid but also formed a +48 derivative that was not detected in the C<sub>P</sub>S mutated form of the enzyme, which is therefore consistent with sulfonic acid formation, and that appears in the monomeric as well as in the dimeric species (Figure 5). The formation of sulfonic acid in Cys<sub>P</sub> of HsPrx3 had already been reported in HsPrx3 not only in vitro but also in vivo under physiological conditions, in the mitochondria from old rats [49].

The rate constants of oxidation of HsPrx3 were similar for every *t*FA-OOHs tested so far (Figure 2), and to those reported for  $H_2O_2$ - and peroxyxynitrite-mediated oxidations (Table 3). However, the rate constants of HsPrx3 hyperoxidation differed in several orders of magnitude: 15(S)-HpETE and 15(S)-HpEPE were the fastest and  $H_2O_2$  was the slowest (Table 3).

**Table 3.** Kinetics of HsPrx3 oxidation and hyperoxidation by biologically relevant hydroperoxides.

Hydroperoxide	$k_{ox}$ . ( $M^{-1}s^{-1}$ )	$k_{hyperox}$ . ( $M^{-1}s^{-1}$ )	Reference
$H_2O_2$	$2.0 \times 10^7$ <sup>(1)</sup>	$6 \times 10^3$ <sup>(1)</sup> ; $1.1 \times 10^3$ <sup>(2)</sup>	[12,13,15]
Peroxyxynitrite	$1.0 \times 10^7$ <sup>(3)</sup>	Not determined	[13]
15(S)-HpEPE	$>3.5 \times 10^7$ <sup>(4)</sup>	$(2.6 \pm 0.4) \times 10^7$ <sup>(4)</sup>	This work
15(S)-HpETE	$>3.5 \times 10^7$ <sup>(4)</sup>	$(1.7 \pm 0.1) \times 10^7$ <sup>(4)</sup>	This work
PGG <sub>2</sub>	$2.4 \times 10^7$ <sup>(4)</sup>	$(3.1 \pm 0.7) \times 10^5$ <sup>(4)</sup>	This work

<sup>(1)</sup> pH 7.4, 25 °C; <sup>(2)</sup> pH 7.8, 14 °C; <sup>(3)</sup> pH 7.8, 25 °C; <sup>(4)</sup> pH 7.8, 11–12 °C. Mean values and standard deviations of the rate constants were calculated from three independent experiments.

These reactivities explain the rapid inactivation of HsPrx3 exposed to 20  $\mu$ M *t*FA-OOH but not to 20  $\mu$ M  $H_2O_2$  as observed in the coupled catalytic assay (Figure 1). Indeed,  $k_{hyperoxidation} \times [ROOH]$  is 520  $s^{-1}$  for 15(S)-HpEPE, 340  $s^{-1}$  for 15(S)-HpETE, 6.2  $s^{-1}$  for PGG<sub>2</sub> and 0.022  $s^{-1}$  for  $H_2O_2$ . Since hyperoxidation competes with resolution ( $2 s^{-1}$ ) for the sulfenic acid in Cys<sub>P</sub> of the oxidized enzyme, expected amounts of hyperoxidized enzyme can be calculated as ~99% for 15(S)-HpEPE, and 15(S)-HpETE, a fraction that decreased to ~70% for PGG<sub>2</sub> and ~1% for  $H_2O_2$  under the conditions employed in Figure 4. Indeed, HsPrx3 hyperoxidation was detected at much lower concentrations of 15(S)-HpEPE, and 15(S)-HpETE than of  $H_2O_2$  and even at equimolar concentrations hyperoxidation at both Cys<sub>P</sub> of the dimeric functional unit of HsPrx3 is detected (as hyperoxidized monomers) (Figure 4). However, there is still a substantial proportion of the enzyme with one Cys<sub>P</sub> bound to Cys<sub>R</sub> (as hyperoxidized dimers) indicating that Cys<sub>P</sub> of HsPrx3 was not ~99% hyperoxidized. This probably reflects active site asymmetry in HsPrx3, a dodecameric enzyme under reduced state [75], as already proposed for this and other members of the Prx family [37,58,74]. In this respect, it was previously reported that only half HsPrx3 active sites were susceptible to hyperoxidation even at very high  $H_2O_2$  concentrations (20 mM), forming hyperoxidized dimers as main products [76]. The slower hyperoxidation rate constant of HsPrx3 by PGG<sub>2</sub> with respect to 15(S)-HpEPE, and 15(S)-HpETE is probably a consequence of its particular structure, since it is an endoperoxide-hydroperoxide, which could affect its interaction with HsPrx3 active site.

Biophysical experiments using ANS showed a dose-dependent quenching of the intrinsic fluorescence of HsPrx3 as well as a blue shift and an increase in ANS quantum yields in the presence of the protein (Figure 6A–C). These data suggest the presence of a hydrophobic region in HsPrx3 accessible from the solvent and with nearby positive charges [61,62]. However, the  $K_a$  value obtained of 0.016  $\mu$ M<sup>-1</sup> is an order of magnitude lower than those reported for fatty acid binding proteins such as bovine serum albumin

( $0.32 \mu\text{M}^{-1}$ ) or even for the 1-Cys Prx from *Mycobacterium tuberculosis* AhpE ( $0.16 \mu\text{M}^{-1}$ ). Indeed, the  $K_a$  value for ANS binding to HsPrx3 is in the range of those attributed to the binding of ANS to molten globule-like states of proteins [77]. Therefore, the existence of a well-defined binding site for hydrophobic compounds such as FA was not unambiguously proven by this technique. The ability of HsPrx3 to bind fatty acids was further analyzed by measuring the effects of AA on the melting temperature of reduced HsPrx3 (Figure 6D) and a model of interaction is proposed based on the results obtained using docking simulations (Figure 7). Indeed, in an inspection of the HsPrx3 dimer structure and dynamics, we found and characterized a hydrophobic patch in close proximity to the enzyme active site that can allocate  $\text{rFA-OOHs}$  in such a way that may assist on their reduction by Cys<sub>P</sub>. It should be taken into account that the binding of  $\text{rFA-OOH}$  to HsPrx3 is not of high affinity, since the non-oxidizable fatty acid palmitic acid did not compete with ANS for the binding to HsPrx3. The effect of low-affinity binding of non-reactive parts of substrates in catalysis was initially described by Jenks and coworkers [78] and is nowadays ascribed at least partially to changes in activation entropy of the reaction [79]. That was indeed the case in the one-cysteine Prx from *Mycobacterium tuberculosis* AhpE, that reacted much faster with  $\text{rFA-OOH}$  than with  $\text{H}_2\text{O}_2$  at the expense of an important increase in the activation entropy of the Cys<sub>P</sub> oxidation reaction [41].

From the kinetics of  $\text{rFA-OOHs}$  reduction by different mitochondrial peroxidases and other potential mitochondrial targets previously and herein reported (Table 4), it emerges that HsPrx3 should be considered a preferential target for these species, particularly of 15(S)-HpETE and 15(S)-HpEPE. This is because of the fast rate constants of reaction combined with the high abundance of the enzyme in many cellular types, with reported concentration values in the 10–120  $\mu\text{M}$  range [13]. In turn, GPx1 is oxidized by FA-OOHs with a similar rate constant ( $4 \times 10^7 \text{ M}^{-1}\text{s}^{-1}$  [28]) but its mitochondrial concentration is lower, so its contribution to  $\text{rFA-OOH}$  reduction is expected to be minor. Data on the kinetics of oxidation of HsPrx5 by  $\text{rFA-OOH}$  are lacking so far, but if the high reactivity of the enzyme with other organic hydroperoxides is maintained ( $\sim 10^7 \text{ M}^{-1}\text{s}^{-1}$ ) [80], then Prx5 would also represent a main target of  $\text{rFA-OOH}$  since its mitochondrial concentration can attain 16  $\mu\text{M}$  [81]. Of course, these calculations rely on the concentrations of the different peroxidases under reduced state, which can decrease if reduction by the mitochondrial reduction systems rate limits catalysis, or if the fraction of inactive enzymes (which includes but is not limited to hyperoxidized protein) increases. Similar calculations cannot be performed for PGG<sub>2</sub> or similar endoperoxide-hydroperoxides since the kinetic data on its reactions with other mitochondrial targets are still lacking.

Previous data indicated a mitochondrial formation flux of  $\text{O}_2^{\bullet-}$  of 0.8  $\mu\text{M/s}$  in endothelial cells under normoglycemia, which can increase almost 10-fold under hyperglycemic conditions [82]. Most of it dismutates to  $\text{H}_2\text{O}_2$  and  $\text{O}_2$  in a reaction catalyzed by Mn-superoxide dismutase (MnSOD), a highly efficient enzyme abundant in the organelle. Other potential targets of  $\text{O}_2^{\bullet-}$  include  $\bullet\text{NO}$ , which depending on its steady-state concentrations, can compete for a fraction of  $\text{O}_2^{\bullet-}$  and form peroxynitrite [4]. In sake of simplicity, we did not include in our simulations formation fluxes of  $\bullet\text{NO}$  which largely vary depending on conditions and cell type [4]. Considering mitochondrial formation fluxes of  $\text{H}_2\text{O}_2$  in the 0.4–4  $\mu\text{M/s}$  range and rate constants and concentrations indicated in Table 4, we determined expected yields of hyperoxidized Prx3 in the mitochondrial matrix as indicated in Table 5. Formation rates of  $\text{rFA-OOH}$  in mitochondrial membranes have been previously estimated as 0.1  $\mu\text{M/s}$  [83]. Estimation of formation rates of  $\text{rFA-OOH}$  in the mitochondrial matrix are lacking, although they have been reported to largely vary under different physiopathological conditions [6]. So, we spanned a three order of magnitude range of  $\text{rFA-OOH}$  formation rates to investigate the expected effects on HsPrx3 hyperoxidation. Time course simulations that were one hour long were performed in order to avoid other variables such as hyperoxidized HsPrx3 sulfinic acid reduction by sulfiredoxin (which requires the translocation of sulfiredoxin, a cytosolic protein, to the mitochondria [84]) as well as protein turnover [85]. Due to the location of cytochrome *c* preferentially as-

sociated to the outer surface of the inner mitochondrial membrane, reduction of  $\text{H}_2\text{O}_2$  ( $4.6 \times 10^1 \text{ M}^{-1}\text{s}^{-1}$ ) or  $\text{fFA-OOH}$  ( $k \sim 10^4 \text{ M}^{-1}\text{s}^{-1}$ ) by cytochrome *c*/cardiolipin complexes [86] were not considered in the simulations related to *HsPrx3* hyperoxidation in the mitochondrial matrix shown in Table 5. However, with a calculated  $t_{1/2}$  value in the ms range ( $t_{1/2} = \ln 2 / \sum k \times [\text{peroxidases}]$ , see Table 4), the diffusion of a fraction of  $\text{fFA-OOH}$  formed in the mitochondrial matrix through the inner mitochondrial membrane to reach the cytochrome *c*/cardiolipin complex, a process that has been reported to be facilitated by particular proteins, is in principle possible. This would be particularly important under conditions of increased oxidative stress, where the fraction of oxidized and hyperoxidized *HsPrx3* increases [87,88].

**Table 4.** Rate constants and concentrations used in simulations of expected yields of *HsPrx3* hyperoxidation.

Reaction	$k$ ( $\text{M}^{-1}\text{s}^{-1}$ or $\text{s}^{-1}$ )	Reference
(1) $\text{redPrx3} + \text{H}_2\text{O}_2 \rightarrow \text{Prx3SOH} + \text{H}_2\text{O}$	$2 \times 10^7$	[12]
(2) $\text{Prx3SOH} \rightarrow \text{Prx3SS}$	2	[13]
(3) $\text{Prx3SOH} + \text{H}_2\text{O}_2 \rightarrow \text{Prx3SO}_2\text{H} + \text{H}_2\text{O}$	$1.1 \times 10^3$	[13]
(4) $\text{redPrx3} + \text{fFA-OOH} \rightarrow \text{Prx3SOH} + \text{fFA-OH}$	$3.5 \times 10^7$	This work
(5) $\text{Prx3SOH} + \text{fFA-OOH} \rightarrow \text{Prx3SO}_2\text{H} + \text{fFA-OH}$	$1 \times 10^7$	This work
(6) $\text{Prx3SS} + \text{redTrx2/Grx2} \rightarrow \text{redPrx3} + \text{oxTrx2/Grx2}$	$4 \times 10^4$ <sup>a</sup>	[54]
(7) $\text{redPrx5} + \text{H}_2\text{O}_2 \rightarrow \text{Prx5SOH} + \text{H}_2\text{O}$	$3 \times 10^5$	[80]
(8) $\text{redPrx5} + \text{fFA-OOH} \rightarrow \text{Prx5SOH} + \text{fFA-OH}$	$2 \times 10^7$ <sup>b</sup>	[80]
(9) $\text{Prx5SOH} \rightarrow \text{Prx5SS}$	15	[80]
(10) $\text{Prx5SS} + \text{redTrx2} \rightarrow \text{redPrx5} + \text{redTrx2}$	$2 \times 10^6$	[80]
(11) $\text{redGPx1}^c + \text{H}_2\text{O}_2 \rightarrow \text{oxGPx1} + \text{H}_2\text{O}$	$4 \times 10^7$	[28]
(12) $\text{redGPx1} + \text{fFA-OOH} \rightarrow \text{oxGPx1} + \text{fFA-OH}$	$4 \times 10^7$	[28]
(13) $\text{oxGPx1} + 2\text{GSH}^d \rightarrow \text{redGPx1} + \text{GSSG}$	$2 \times 10^5$	[28]

<sup>a</sup> The rate constant of Prx3 disulfide (Prx3SS) reduction by the physiological reducing substrates Trx2 and/or Grx2 was set as  $4 \times 10^4 \text{ M}^{-1}\text{s}^{-1}$  as estimated from the catalytic efficiency ( $k_{\text{cat}}/K_m$ ) values reported in [54]. Trx2 plus Grx2 concentration in mitochondria was assumed to sum  $10 \mu\text{M}$  [12] and was fixed under reduced state in the simulations (reduction of the redoxins is not rate limiting peroxide consumption). The concentration of Trx2 and Grx2 varies with the cellular type [54]. <sup>b</sup> The kinetics of the reactions of reduced *HsPrx5* with FA-OOHs is unknown so far. In these simulations, we assumed a rate constant similar to those of the enzyme oxidation by the non-natural organic hydroperoxides *tert*-butyl hydroperoxide and cumene hydroperoxides reported in [80]. The concentration of Prx5 was set as  $16 \mu\text{M}$  as reported in [89]. The susceptibility of *HsPrx5* to hyperoxidation was reported to be low, so we did not include it in the simulations [90]. <sup>c</sup> Mitochondria express GPx1 with a concentration  $\sim 2 \mu\text{M}$  [91]. Although GPx4 can also be expressed in the mitochondria, particularly in testis, its expression levels are low in most somatic tissues and therefore it was not included in the simulations [30]. <sup>d</sup> Glutathione concentration was set at  $5 \text{ mM}$  and was fixed under reduced state, i.e., in these simulations it is assumed that reduction of glutathione by glutathione reductase/NADPH is faster than glutathione oxidation.

Under low physiological mitochondrial fluxes of  $\text{H}_2\text{O}_2$  of  $\sim 0.4 \mu\text{M/s}$ , the amount of hyperoxidized *HsPrx3* formed in the mitochondrial matrix in one hour is  $\leq 1 \text{ nM}$ , unless a concomitant flux of  $\text{fFA-OOH}$  in the order of  $0.001\text{--}0.1 \mu\text{M/s}$  occurs. On the contrary, at higher fluxes of  $\text{H}_2\text{O}_2$  formation such as  $4 \mu\text{M/s}$ , hyperoxidized enzyme can reach  $\sim 10\text{--}100 \text{ nM}$  levels in the absence of fluxes of  $\text{fFA-OOH}$ , but still the latter are required for a significant fraction ( $\geq 1\%$ ) of the enzyme to be hyperoxidized in an hour. For example, for 2% hyperoxidation of the enzyme in an hour, a concomitant flux of  $0.1 \mu\text{M/s}$  of  $\text{fFA-OOH}$  is needed in mitochondria expressing  $100 \mu\text{M}$  *HsPrx3*. In mitochondria expressing  $20 \mu\text{M}$  *HsPrx3* formation rates of  $\text{fFA-OOH}$  required for a similar percentage of *HsPrx3* inactivation are in the  $\text{nM/s}$  range (Table 5). Thus, our results indicate that mitochondrial  $\text{fFA-OOH}$  contributes to the inactivation through hyperoxidation of *HsPrx3*, a modification that has been detected in cells under both physiological and pathological conditions [49,50,92–94].

Similar data regarding the oxidation and hyperoxidation of the cytosolic Prx1 and Prx2 by  $\text{fFA-OOH}$  are lacking so far, with the only exception of the initial report by Cha et al. [34]. The peroxidatic active site in the three Prxs is highly conserved. More interestingly, all the residues that make up the hydrophobic patch in *HsPrx3* (Figure 7) are conserved in Prx2 (Supplementary Figure S5). Furthermore, the reported rate constants of oxidation and hyperoxidation by  $\text{H}_2\text{O}_2$  are similar [13,59,95,96]. Thus, it is tempting to speculate

that the rate constants of oxidation and hyperoxidation by FA-OOH would probably be also similar, differences in susceptibility to hyperoxidation arising from differences in rates constants of resolution as in the case of H<sub>2</sub>O<sub>2</sub>. If that is the case, and since Prx2 is the one with the lower resolution rate constant, it would be expected to be the enzyme more prone to hyperoxidation also by fFA-OOH among the three. This is very interesting due to the different cellular compartmentalization of Prx2 (mostly cytosolic) with respect to Prx3 and due to the fact that depending on cells and conditions, fFA-OOH can be preferentially formed in different cell compartments. However, future work is required to test this hypothesis.

Prxs and particularly, typical 2-Cys Prxs participate in redox signaling actions through different mechanisms. In the flood gate mechanism of redox signaling, hyperoxidation and the consequent inactivation of Prxs would allow the oxidation of other, less reactive hydroperoxide targets [97]. In the redox relay mechanism, Prxs act as sensors of hydroperoxides transferring the oxidation to signaling proteins [98,99]. We propose that HsPrx3 oxidation and hyperoxidation by fFA-OOH reported herein contribute to both signaling mechanisms, either by increasing enzyme hyperoxidation yields but also serving as sensors of fFA-OOH in mitochondria.

**Table 5.** Expected percentages of hyperoxidated HsPrx3 in mitochondria forming different fluxes of H<sub>2</sub>O<sub>2</sub> and fFAOOH.

% of Prx3-SO <sub>2</sub> <sup>-</sup> with Respect to Initial Reduced Prx3				
[Reduced Prx3] 20 μM <sup>a</sup>				
fFA-OOH (μM/s)	H <sub>2</sub> O <sub>2</sub> (μM/s)	0.4	1	4
0		$2.8 \times 10^{-3}$	$2 \times 10^{-2}$	0.37
0.001		$3.3 \times 10^{-2}$	0.1	0.75
0.01		0.30	0.8	4
0.1		3.7	8.5	39
[Reduced Prx3] 100 μM <sup>a</sup>				
fFA-OOH (μM/s)	H <sub>2</sub> O <sub>2</sub> (μM/s)	0.4	1	4
0		$1.5 \times 10^{-4}$	$9.3 \times 10^{-4}$	$1.6 \times 10^{-2}$
0.001		$2.0 \times 10^{-3}$	$5.6 \times 10^{-3}$	$3.6 \times 10^{-2}$
0.01		$1.9 \times 10^{-2}$	$4.8 \times 10^{-2}$	0.22
0.1		0.23	0.51	2.1

<sup>a</sup> Two different concentrations of Prx3 were included in the simulations, which are in the lower and higher range of those reported in the literature [12,14,100,101].

## 5. Conclusions

Herein, we demonstrate that HsPrx3 is rapidly oxidized and hyperoxidized by fFA-OOH, with rate constants that are in the order of  $\geq 3.5 \times 10^7$  and  $\sim 10^7 \text{ M}^{-1}\text{s}^{-1}$  for the AA-derived 15(S)-HpETE and EPA-derived 15(S)-HpEPE, respectively. Compared with other biologically relevant hydroperoxides such as H<sub>2</sub>O<sub>2</sub> and peroxynitrite, the rate constants of HsPrx3 oxidation by these fFA-OOHs are in the same order of magnitude, but hyperoxidation rate constants are considerably higher (Table 3). The endoperoxide-hydroperoxide PGG<sub>2</sub>, also derived from AA, oxidized HsPrx3 almost as rapidly but showed a lower rate constant of hyperoxidation. We present a model of interaction of fFA-OOH with HsPrx3 in which the former binds to a hydrophobic patch of the enzyme and positions the hydroperoxide group in close proximity to Cys<sub>P</sub> that would facilitate the reaction. We propose that, as for other mitochondrial hydroperoxides such as H<sub>2</sub>O<sub>2</sub> and peroxynitrite, HsPrx3 is expected to be a main target for fFA-OOH at least under low oxidative stress conditions in which most of the enzyme is under reduced state. Finally, our results indicate that low fluxes of fFA-OOHs (in the nM/s range) formed in the mitochondrial matrix are expected to increase hyperoxidation yields of HsPrx3 in mitochondria under different conditions. Considering the key roles of Prxs in redox signaling processes we propose HsPrx3 not only as a reductant but also as a sensor of fFA-OOHs formed in mitochondria.

**Supplementary Materials:** The following supporting information can be downloaded at: <https://www.mdpi.com/article/10.3390/antiox12020408/s1>, Figure S1: Molecular representations of fFA-OOH and FA used throughout this work. Figure S2: Intrinsic fluorescence changes in HsPrx3 caused by CysP oxidation, resolution and hyperoxidation. Figure S3: Effect of 15(S)-HpETE versus H<sub>2</sub>O<sub>2</sub> on the distribution of HsPrx3 between monomeric and disulfide-bonded dimeric species. Figure S4: Effect of ethanol on the heat-induced unfolding of HsPrx3. Figure S5: Sequence alignment of HsPrx3 and HsPrx2.

**Author Contributions:** Conceptualization and design, M.T. and A.M.R. G.C. made most of the experiments. G.C. and M.M. made the experiments related to mass spectrometry and A.Z. the molecular dynamic simulations and docking. N.V. and M.T. made the simulations of expected hyperoxidation yields. All authors discussed the results obtained. M.T., A.M.R., A.Z., R.R. and G.C. wrote and edited the manuscript. All authors have read and agreed to the published version of the manuscript.

**Funding:** This work was supported by grants from Comisión Sectorial de Investigación Científica (I+D 2020 to A.M.R. and M.T., CSIC\_2018 to R.R.) and Espacio Interdisciplinario\_2020 (to R.R.), Universidad de la República, Uruguay. Additional support was obtained from Programa de Desarrollo de Ciencias Básicas (PEDECIBA, Uruguay), Sistema Nacional de Investigadores (SNI, Uruguay) and Programa de Alimentos y Salud Humana (PAYS) IDB—R.O.U. (4950/OC-UR).

**Informed Consent Statement:** Not applicable.

**Data Availability Statement:** The data are contained within this article.

**Acknowledgments:** We thank Lucía Turell from Facultad de Ciencias, Universidad de la República and Mariana Bonilla, Institut Pasteur Montevideo, Uruguay, for kindly providing the plasmids for recombinant expression of EgTR. We also thank Bruno Manta, Universidad de la República and Institut Pasteur Montevideo for providing the plasmid for recombinant expression of HsTrx1. The molecular simulations presented herein were carried out using ClusterUY [102].

**Conflicts of Interest:** The authors declare no conflict of interest.

## Abbreviations

Hydrogen peroxide, H<sub>2</sub>O<sub>2</sub>; fatty acid, FA; free fatty acid hydroperoxide, fFA-OOH; lipid-bound fatty acid hydroperoxide, lFA-OOH; peroxiredoxins, Prxs; peroxidatic cysteine, Cys<sub>P</sub>, resolving cysteine, Cys<sub>R</sub>; polyunsaturated fatty acids, PUFA; linoleic acid, LA; arachidonic acid, AA; eicosapentaenoic acid, EPA; glutathione peroxidase, GPx; human Prx3, HsPrx3; 15S-hydroperoxy-5Z,8Z,11Z,13E-eicosatetraenoic acid, 15(S)-HpETE; 15S-hydroperoxy-5Z,8Z,11Z,13E,17Z-eicosapentaenoic acid, 15(S)-HpEPE; 9 $\alpha$ ,11 $\alpha$ -epidioxy-15S-hydroperoxy-prosta-5Z,13E-dien-1-oic acid, PGG<sub>2</sub>; dithiotreitol, DTT; N-ethylmaleimide, NEM; beta-mercaptoethanol,  $\beta$ -ME; reduced nicotinamide adenine dinucleotide phosphate, NADPH; isopropyl- $\beta$ -D-thiogalactopyranoside, IPTG; diethylenetriaminepentaacetic acid, DTPA; 8-anilino-1-naphthalene sulfonic acid, ANS; human thioredoxin 1, HsTrx1; *Echinococcus granulosus* thioredoxin glutathione reductase, EgTR; Cys<sub>P</sub> to Ser mutated form of human Prx3, C<sub>P</sub>SHsPrx3; Observed rate constant,  $k_{obs}$ ; fluorescence resonance energy transfer, FRET; molecular dynamic, MD; mass spectrometry, MS; carbamidomethyl, CAM.

## References

1. Murphy, M.P. How mitochondria produce reactive oxygen species. *Biochem. J.* **2009**, *417*, 1–13. [[CrossRef](#)] [[PubMed](#)]
2. Zhang, B.; Pan, C.; Feng, C.; Yan, C.; Yu, Y.; Chen, Z.; Guo, C.; Wang, X. Role of mitochondrial reactive oxygen species in homeostasis regulation. *Redox Rep.* **2022**, *27*, 45–52. [[CrossRef](#)] [[PubMed](#)]
3. Sies, H. Hydrogen peroxide as a central redox signaling molecule in physiological oxidative stress: Oxidative eustress. *Redox Biol.* **2017**, *11*, 613–619. [[CrossRef](#)]
4. Piacenza, L.; Zeida, A.; Trujillo, M.; Radi, R. The superoxide radical switch in the biology of nitric oxide and peroxyntirite. *Physiol. Rev.* **2022**, *102*, 1881–1906. [[CrossRef](#)]
5. Mauerhofer, C.; Philippova, M.; Oskolkova, O.V.; Bochkov, V.N. Hormetic and anti-inflammatory properties of oxidized phospholipids. *Mol. Asp. Med.* **2016**, *49*, 78–90. [[CrossRef](#)] [[PubMed](#)]

6. Bhattacharya, A.; Muller, F.L.; Liu, Y.; Sabia, M.; Liang, H.; Song, W.; Jang, Y.C.; Ran, Q.; Van Remmen, H. Denervation induces cytosolic phospholipase A2-mediated fatty acid hydroperoxide generation by muscle mitochondria. *J. Biol. Chem.* **2009**, *284*, 46–55. [[CrossRef](#)] [[PubMed](#)]
7. Ademowo, O.S.; Dias, H.; Burton, D.G.; Griffiths, H.R. Lipid (per) oxidation in mitochondria: An emerging target in the ageing process? *Biogerontology* **2017**, *18*, 859–879. [[CrossRef](#)] [[PubMed](#)]
8. Peoples, J.N.; Saraf, A.; Ghazal, N.; Pham, T.T.; Kwong, J.Q. Mitochondrial dysfunction and oxidative stress in heart disease. *Exp. Mol. Med.* **2019**, *51*, 1–13. [[CrossRef](#)] [[PubMed](#)]
9. Jomova, K.; Vondrakova, D.; Lawson, M.; Valko, M. Metals, oxidative stress and neurodegenerative disorders. *Mol. Cell. Biochem.* **2010**, *345*, 91–104. [[CrossRef](#)] [[PubMed](#)]
10. Fisher-Wellman, K.H.; Neuffer, P.D. Linking mitochondrial bioenergetics to insulin resistance via redox biology. *Trends Endocrinol. Metab.* **2012**, *23*, 142–153. [[CrossRef](#)] [[PubMed](#)]
11. Quijano, C.; Trujillo, M.; Castro, L.; Trostchansky, A. Interplay between oxidant species and energy metabolism. *Redox Biol.* **2016**, *8*, 28–42. [[CrossRef](#)]
12. Cox, A.G.; Winterbourn, C.C.; Hampton, M.B. Mitochondrial peroxiredoxin involvement in antioxidant defence and redox signalling. *Biochem. J.* **2010**, *425*, 313–325. [[CrossRef](#)] [[PubMed](#)]
13. De Armas, M.I.; Esteves, R.; Viera, N.; Reyes, A.M.; Mastrogiovanni, M.; Alegria, T.G.P.; Netto, L.E.S.; Tortora, V.; Radi, R.; Trujillo, M. Rapid peroxynitrite reduction by human peroxiredoxin 3: Implications for the fate of oxidants in mitochondria. *Free. Radic. Biol. Med.* **2019**, *130*, 369–378. [[CrossRef](#)] [[PubMed](#)]
14. Cox, A.G.; Pearson, A.G.; Pullar, J.M.; Jönsson, T.J.; Lowther, W.T.; Winterbourn, C.C.; Hampton, M.B. Mitochondrial peroxiredoxin 3 is more resilient to hyperoxidation than cytoplasmic peroxiredoxins. *Biochem. J.* **2009**, *421*, 51–58. [[CrossRef](#)] [[PubMed](#)]
15. Peskin, A.V.; Pace, P.E.; Winterbourn, C.C. Enhanced hyperoxidation of peroxiredoxin 2 and peroxiredoxin 3 in the presence of bicarbonate/CO<sub>2</sub>. *Free. Radic. Biol. Med.* **2019**, *145*, 1–7. [[CrossRef](#)] [[PubMed](#)]
16. Angelova, P.R.; Esteras, N.; Abramov, A.Y. Mitochondria and lipid peroxidation in the mechanism of neurodegeneration: Finding ways for prevention. *Med. Res. Rev.* **2021**, *41*, 770–784. [[CrossRef](#)] [[PubMed](#)]
17. Kagan, V.E.; Tyurin, V.A.; Jiang, J.; Tyurina, Y.Y.; Ritov, V.B.; Amoscato, A.A.; Osipov, A.N.; Belikova, N.A.; Kapralov, A.A.; Kini, V. Cytochrome c acts as a cardiolipin oxygenase required for release of proapoptotic factors. *Nat. Chem. Biol.* **2005**, *1*, 223–232. [[CrossRef](#)]
18. Colbeau, A.; Nachbaur, J.; Vignais, P. Enzymatic characterization and lipid composition of rat liver subcellular membranes. *Biochim. Et Biophys. Acta (BBA)-Biomembr.* **1971**, *249*, 462–492. [[CrossRef](#)]
19. Belikova, N.A.; Vladimirov, Y.A.; Osipov, A.N.; Kapralov, A.A.; Tyurin, V.A.; Potapovich, M.V.; Basova, L.V.; Peterson, J.; Kurnikov, I.V.; Kagan, V.E. Peroxidase activity and structural transitions of cytochrome c bound to cardiolipin-containing membranes. *Biochemistry* **2006**, *45*, 4998–5009. [[CrossRef](#)]
20. Ježek, J.; Dlasková, A.; Zelenka, J.; Jabůrek, M.; Ježek, P. H<sub>2</sub>O<sub>2</sub>-activated mitochondrial phospholipase iPLA<sub>2</sub>γ prevents lipotoxic oxidative stress in synergy with UCP2, amplifies signaling via G-protein-coupled receptor GPR40, and regulates insulin secretion in pancreatic β-cells. *Antioxid. Redox Signal.* **2015**, *23*, 958–972. [[CrossRef](#)]
21. Průchová, P.; Gotvaldová, K.; Smolková, K.; Alán, L.; Holendová, B.; Tauber, J.; Galkin, A.; Ježek, P.; Jabůrek, M. Antioxidant Role and Cardiolipin Remodeling by Redox-Activated Mitochondrial Ca<sup>2+</sup>-Independent Phospholipase A<sub>2</sub>γ in the Brain. *Antioxidants* **2022**, *11*, 198. [[CrossRef](#)] [[PubMed](#)]
22. Ježek, J.; Jabůrek, M.; Zelenka, J.; Ježek, P. Mitochondrial phospholipase A<sub>2</sub> activated by reactive oxygen species in heart mitochondria induces mild uncoupling. *Physiol. Res.* **2010**, *59*, 737–747. [[CrossRef](#)] [[PubMed](#)]
23. Pallast, S.; Arai, K.; Wang, X.; Lo, E.H.; Van Leyen, K. 12/15-Lipoxygenase targets neuronal mitochondria under oxidative stress. *J. Neurochem.* **2009**, *111*, 882–889. [[CrossRef](#)] [[PubMed](#)]
24. Dixon, S.J.; Lemberg, K.M.; Lamprecht, M.R.; Skouta, R.; Zaitsev, E.M.; Gleason, C.E.; Patel, D.N.; Bauer, A.J.; Cantley, A.M.; Yang, W.S. Ferroptosis: An iron-dependent form of nonapoptotic cell death. *Cell* **2012**, *149*, 1060–1072. [[CrossRef](#)]
25. Lane, D.J.; Ayton, S.; Bush, A.I. Iron and Alzheimer’s disease: An update on emerging mechanisms. *J. Alzheimer’s Dis.* **2018**, *64*, S379–S395. [[CrossRef](#)]
26. Zhang, J.; Shi, Y. In Search of the Holy Grail: Toward a Unified Hypothesis on Mitochondrial Dysfunction in Age-Related Diseases. *Cells* **2022**, *11*, 1906. [[CrossRef](#)]
27. Schuckelt, R.; Brigelius-Flohe, R.; Maiorino, M.; Roveri, A.; Reumkens, J.; Strabburger, W.; Ursini, F.; Wolf, B.; Flohe, L. Phospholipid hydroperoxide glutathione peroxidase is a seleno-enzyme distinct from the classical glutathione peroxidase as evident from cDNA and amino acid sequencing. *Free. Radic. Res. Commun.* **1991**, *14*, 343–361. [[CrossRef](#)]
28. Toppo, S.; Flohé, L.; Ursini, F.; Vanin, S.; Maiorino, M. Catalytic mechanisms and specificities of glutathione peroxidases: Variations of a basic scheme. *Biochim. Et Biophys. Acta (BBA)-Gen. Subj.* **2009**, *1790*, 1486–1500. [[CrossRef](#)]
29. Yant, L.J.; Ran, Q.; Rao, L.; Van Remmen, H.; Shibatani, T.; Belter, J.G.; Motta, L.; Richardson, A.; Prolla, T.A. The selenoprotein GPX4 is essential for mouse development and protects from radiation and oxidative damage insults. *Free. Radic. Biol. Med.* **2003**, *34*, 496–502. [[CrossRef](#)]
30. Schneider, M.; Forster, H.; Boersma, A.; Seiler, A.; Wehnes, H.; Sinowatz, F.; Neumuller, C.; Deutsch, M.J.; Walch, A.; Hrabe de Angelis, M.; et al. Mitochondrial glutathione peroxidase 4 disruption causes male infertility. *FASEB J.* **2009**, *23*, 3233–3242. [[CrossRef](#)]

31. Maiorino, M.; Roveri, A.; Benazzi, L.; Bosello, V.; Mauri, P.; Toppo, S.; Tosatto, S.C.; Ursini, F. Functional interaction of phospholipid hydroperoxide glutathione peroxidase with sperm mitochondrion-associated cysteine-rich protein discloses the adjacent cysteine motif as a new substrate of the selenoperoxidase. *J. Biol. Chem.* **2005**, *280*, 38395–38402. [[CrossRef](#)]
32. Azuma, K.; Koumura, T.; Iwamoto, R.; Matsuoka, M.; Terauchi, R.; Yasuda, S.; Shiraya, T.; Watanabe, S.; Aihara, M.; Imai, H. Mitochondrial glutathione peroxidase 4 is indispensable for photoreceptor development and survival in mice. *J. Biol. Chem.* **2022**, *298*, 4. [[CrossRef](#)] [[PubMed](#)]
33. Flohé, L.; Toppo, S.; Cozza, G.; Ursini, F. A comparison of thiol peroxidase mechanisms. *Antioxid. Redox Signal.* **2011**, *15*, 763–780. [[CrossRef](#)] [[PubMed](#)]
34. Cha, M.-K.; Yun, C.-H.; Kim, I.-H. Interaction of human thiol-specific antioxidant protein 1 with erythrocyte plasma membrane. *Biochemistry* **2000**, *39*, 6944–6950. [[CrossRef](#)] [[PubMed](#)]
35. Li, H.; Benipal, B.; Zhou, S.; Dodia, C.; Chatterjee, S.; Tao, J.-Q.; Sorokina, E.M.; Raabe, T.; Feinstein, S.I.; Fisher, A.B. Critical role of peroxiredoxin 6 in the repair of peroxidized cell membranes following oxidative stress. *Free. Radic. Biol. Med.* **2015**, *87*, 356–365. [[CrossRef](#)] [[PubMed](#)]
36. Schlecker, T.; Schmidt, A.; Dirdjaja, N.; Voncken, F.; Clayton, C.; Krauth-Siegel, R.L. Substrate specificity, localization, and essential role of the glutathione peroxidase-type trypanoxin peroxidases in *Trypanosoma brucei*. *J. Biol. Chem.* **2005**, *280*, 14385–14394. [[CrossRef](#)]
37. Budde, H.; Flohé, L.; Hecht, H.-J.; Hofmann, B.; Stehr, M.; Wissing, J.; Lünsdorf, H. Kinetics and redox-sensitive oligomerisation reveal negative subunit cooperativity in trypanoxin peroxidase of *Trypanosoma brucei brucei*. *De Gruyter* **2003**. [[CrossRef](#)]
38. Jaeger, T.; Budde, H.; Flohé, L.; Menge, U.; Singh, M.; Trujillo, M.; Radi, R. Multiple thioredoxin-mediated routes to detoxify hydroperoxides in *Mycobacterium tuberculosis*. *Arch. Biochem. Biophys.* **2004**, *423*, 182–191. [[CrossRef](#)]
39. Reyes, A.M.; Hugo, M.; Trostchansky, A.; Capece, L.; Radi, R.; Trujillo, M. Oxidizing substrate specificity of *Mycobacterium tuberculosis* alkyl hydroperoxide reductase E: Kinetics and mechanisms of oxidation and overoxidation. *Free. Radic. Biol. Med.* **2011**, *51*, 464–473. [[CrossRef](#)]
40. Reyes, A.M.; Vazquez, D.S.; Zeida, A.; Hugo, M.; Piñeyro, M.D.; De Armas, M.I.; Estrin, D.; Radi, R.; Santos, J.; Trujillo, M. PrxQ B from *Mycobacterium tuberculosis* is a monomeric, thioredoxin-dependent and highly efficient fatty acid hydroperoxide reductase. *Free. Radic. Biol. Med.* **2016**, *101*, 249–260. [[CrossRef](#)]
41. Zeida, A.; Reyes, A.M.; Lichtig, P.; Hugo, M.; Vazquez, D.S.; Santos, J.; González Flecha, F.L.; Radi, R.; Estrin, D.A.; Trujillo, M. Molecular basis of hydroperoxide specificity in peroxiredoxins: The case of AhpE from *Mycobacterium tuberculosis*. *Biochemistry* **2015**, *54*, 7237–7247. [[CrossRef](#)] [[PubMed](#)]
42. Zhang, Y.; Park, J.; Han, S.-J.; Lim, Y.; Park, I.; Kim, J.-S.; Woo, H.; Lee, S.-R. Peroxiredoxin III protects tumor suppressor PTEN from oxidation by 15-Hydroperoxy-eicosatetraenoic acid. *Oxidative Med. Cell. Longev.* **2019**, *2019*, 2828493. [[CrossRef](#)] [[PubMed](#)]
43. Cordray, P.; Doyle, K.; Edes, K.; Moos, P.J.; Fitzpatrick, F.A. Oxidation of 2-Cys-peroxiredoxins by arachidonic acid peroxide metabolites of lipoxygenases and cyclooxygenase-2. *J. Biol. Chem.* **2007**, *282*, 32623–32629. [[CrossRef](#)] [[PubMed](#)]
44. Bhattacharya, A.; Lustgarten, M.; Shi, Y.; Liu, Y.; Jang, Y.C.; Pulliam, D.; Jernigan, A.L.; Van Remmen, H. Increased mitochondrial matrix-directed superoxide production by fatty acid hydroperoxides in skeletal muscle mitochondria. *Free. Radic. Biol. Med.* **2011**, *50*, 592–601. [[CrossRef](#)] [[PubMed](#)]
45. Whitaker, H.; Patel, D.; Howat, W.; Warren, A.; Kay, J.; Sangan, T.; Marioni, J.; Mitchell, J.; Aldridge, S.; Luxton, H. Peroxiredoxin-3 is overexpressed in prostate cancer and promotes cancer cell survival by protecting cells from oxidative stress. *Br. J. Cancer* **2013**, *109*, 983–993. [[CrossRef](#)] [[PubMed](#)]
46. Chen, X.; Song, X.; Li, J.; Zhang, R.; Yu, C.; Zhou, Z.; Liu, J.; Liao, S.; Klionsky, D.J.; Kroemer, G. Identification of HPCAL1 as a specific autophagy receptor involved in ferroptosis. *Autophagy* **2023**, *19*, 54–74. [[CrossRef](#)]
47. Ingold, I.; Berndt, C.; Schmitt, S.; Doll, S.; Poschmann, G.; Buday, K.; Roveri, A.; Peng, X.; Freitas, F.P.; Seibt, T. Selenium utilization by GPX4 is required to prevent hydroperoxide-induced ferroptosis. *Cell* **2018**, *172*, 409–422.e421. [[CrossRef](#)]
48. Evans, R.C.; Chen, L.; Na, R.; Yoo, K.; Ran, Q. The Gpx4NIKO Mouse Is a Versatile Model for Testing Interventions Targeting Ferroptotic Cell Death of Spinal Motor Neurons. *Neurotox. Res.* **2022**, *40*, 373–383. [[CrossRef](#)]
49. Musicco, C.; Capelli, V.; Pesce, V.; Timperio, A.M.; Calvani, M.; Mosconi, L.; Zolla, L.; Cantatore, P.; Gadaleta, M.N. Accumulation of overoxidized Peroxiredoxin III in aged rat liver mitochondria. *Biochim. Et Biophys. Acta BBA Bioenerg.* **2009**, *1787*, 890–896. [[CrossRef](#)]
50. Kil, I.S.; Lee, S.K.; Ryu, K.W.; Woo, H.A.; Hu, M.-C.; Bae, S.H.; Rhee, S.G. Feedback control of adrenal steroidogenesis via H<sub>2</sub>O<sub>2</sub>-dependent, reversible inactivation of peroxiredoxin III in mitochondria. *Mol. Cell* **2012**, *46*, 584–594. [[CrossRef](#)]
51. Claiborne, A.; Miller, H.; Parsonage, D.; Ross, R.P. Protein-sulfenic acid stabilization and function in enzyme catalysis and gene regulation. *FASEB J.* **1993**, *7*, 1483–1490. [[CrossRef](#)]
52. Jiang, Z.-Y.; Hunt, J.V.; Wolff, S.P. Ferrous ion oxidation in the presence of xylenol orange for detection of lipid hydroperoxide in low density lipoprotein. *Anal. Biochem.* **1992**, *202*, 384–389. [[CrossRef](#)]
53. Cuevasanta, E.; Reyes, A.M.; Zeida, A.; Mastrogiovanni, M.; De Armas, M.I.; Radi, R.; Alvarez, B.; Trujillo, M. Kinetics of formation and reactivity of the persulfide in the one-cysteine peroxiredoxin from *Mycobacterium tuberculosis*. *J. Biol. Chem.* **2019**, *294*, 13593–13605. [[CrossRef](#)] [[PubMed](#)]

54. Hanschmann, E.-M.; Lönn, M.E.; Schütte, L.D.; Funke, M.; Godoy, J.R.; Eitner, S.; Hudemann, C.; Lillig, C.H. Both thioredoxin 2 and glutaredoxin 2 contribute to the reduction of the mitochondrial 2-Cys peroxiredoxin Prx3. *J. Biol. Chem.* **2010**, *285*, 40699–40705. [[CrossRef](#)] [[PubMed](#)]
55. Manta, B.; Hugo, M.; Ortiz, C.; Ferrer-Sueta, G.; Trujillo, M.; Denicola, A. The peroxidase and peroxynitrite reductase activity of human erythrocyte peroxiredoxin 2. *Arch. Biochem. Biophys.* **2009**, *484*, 146–154. [[CrossRef](#)] [[PubMed](#)]
56. Bonilla, M.; Denicola, A.; Novoselov, S.V.; Turanov, A.A.; Protasio, A.; Izmendi, D.; Gladyshev, V.N.; Salinas, G. Platyhelminth mitochondrial and cytosolic redox homeostasis is controlled by a single thioredoxin glutathione reductase and dependent on selenium and glutathione. *J. Biol. Chem.* **2008**, *283*, 17898–17907. [[CrossRef](#)] [[PubMed](#)]
57. Nelson, K.J.; Parsonage, D. Measurement of peroxiredoxin activity. *Curr. Protoc. Toxicol.* **2011**, *49*, 7.10.1–7.10.28. [[CrossRef](#)]
58. Peskin, A.V.; Meotti, F.C.; de Souza, L.F.; Anderson, R.F.; Winterbourn, C.C.; Salvador, A. Intra-dimer cooperativity between the active site cysteines during the oxidation of peroxiredoxin 2. *Free Radic. Biol. Med.* **2020**, *158*, 115–125. [[CrossRef](#)]
59. Portillo-Ledesma, S.; Randall, L.M.; Parsonage, D.; Dalla Rizza, J.; Karplus, P.A.; Poole, L.B.; Denicola, A.; Ferrer-Sueta, G. Differential kinetics of two-cysteine peroxiredoxin disulfide formation reveal a novel model for peroxide sensing. *Biochemistry* **2018**, *57*, 3416–3424. [[CrossRef](#)] [[PubMed](#)]
60. Parsonage, D.; Nelson, K.J.; Ferrer-Sueta, G.; Alley, S.; Karplus, P.A.; Furdui, C.M.; Poole, L.B. Dissecting peroxiredoxin catalysis: Separating binding, peroxidation, and resolution for a bacterial AhpC. *Biochemistry* **2015**, *54*, 1567–1575. [[CrossRef](#)]
61. Cardamone, M.; Puri, N. Spectrofluorimetric assessment of the surface hydrophobicity of proteins. *Biochem. J.* **1992**, *282*, 589–593. [[CrossRef](#)] [[PubMed](#)]
62. Matulis, D.; Lovrien, R. 1-Anilino-8-naphthalene sulfonate anion-protein binding depends primarily on ion pair formation. *Biophys. J.* **1998**, *74*, 422–429. [[CrossRef](#)] [[PubMed](#)]
63. Chang, L.-s.; Wen, E.-y.; Hung, J.-j.; Chang, C.-c. Energy transfer from tryptophan residues of proteins to 8-anilino-1-naphthalene-sulfonate. *J. Protein Chem.* **1994**, *13*, 635–640. [[CrossRef](#)]
64. Das, A.; Basak, P.; Pattanayak, R.; Kar, T.; Majumder, R.; Pal, D.; Bhattacharya, A.; Bhattacharyya, M.; Banik, S.P. Trehalose induced structural modulation of Bovine Serum Albumin at ambient temperature. *Int. J. Biol. Macromol.* **2017**, *105*, 645–655. [[CrossRef](#)]
65. Jorgensen, W.L.; Chandrasekhar, J.; Madura, J.D.; Impey, R.W.; Klein, M.L. Comparison of simple potential functions for simulating liquid water. *J. Chem. Phys.* **1983**, *79*, 926–935. [[CrossRef](#)]
66. Maier, J.A.; Martinez, C.; Kasavajhala, K.; Wickstrom, L.; Hauser, K.E.; Simmerling, C. ff14SB: Improving the accuracy of protein side chain and backbone parameters from ff99SB. *J. Chem. Theory Comput.* **2015**, *11*, 3696–3713. [[CrossRef](#)] [[PubMed](#)]
67. Case, D.A.; Cheatham, T.E., III; Darden, T.; Gohlke, H.; Luo, R.; Merz, K.M., Jr.; Onufriev, A.; Simmerling, C.; Wang, B.; Woods, R.J. The Amber biomolecular simulation programs. *J. Comput. Chem.* **2005**, *26*, 1668–1688. [[CrossRef](#)]
68. Morris, G.M.; Huey, R.; Lindstrom, W.; Sanner, M.F.; Belew, R.K.; Goodsell, D.S.; Olson, A.J. AutoDock4 and AutoDockTools4: Automated docking with selective receptor flexibility. *J. Comput. Chem.* **2009**, *30*, 2785–2791. [[CrossRef](#)] [[PubMed](#)]
69. Suttapitugsakul, S.; Xiao, H.; Smeekens, J.; Wu, R. Evaluation and optimization of reduction and alkylation methods to maximize peptide identification with MS-based proteomics. *Mol. Biosyst.* **2017**, *13*, 2574–2582. [[CrossRef](#)] [[PubMed](#)]
70. Messineo, F.; Pinto, P.; Katz, A. Palmitic acid enhances calcium sequestration by isolated sarcoplasmic reticulum. *J. Mol. Cell. Cardiol.* **1980**, *12*, 725–732. [[CrossRef](#)] [[PubMed](#)]
71. Pompeia, C.; Lima, T.; Curi, R. Arachidonic acid cytotoxicity: Can arachidonic acid be a physiological mediator of cell death? *Cell Biochem. Funct. Cell. Biochem. Its Modul. Act. Agents Dis.* **2003**, *21*, 97–104. [[CrossRef](#)] [[PubMed](#)]
72. Serth, J.; Lautwein, A.; Frech, M.; Wittinghofer, A.; Pingoud, A. The inhibition of the GTPase activating protein-Ha-ras interaction by acidic lipids is due to physical association of the C-terminal domain of the GTPase activating protein with micellar structures. *EMBO J.* **1991**, *10*, 1325–1330. [[CrossRef](#)]
73. Scott, D.E.; Spry, C.; Abell, C. Differential scanning fluorimetry as part of a biophysical screening cascade. In *Fragment-Based Drug Discovery: Lessons and Outlook*; Wiley-VCH: Weinheim, Germany, 2016.
74. Peskin, A.V.; Low, F.M.; Paton, L.N.; Maghzal, G.J.; Hampton, M.B.; Winterbourn, C.C. The high reactivity of peroxiredoxin 2 with H<sub>2</sub>O<sub>2</sub> is not reflected in its reaction with other oxidants and thiol reagents. *J. Biol. Chem.* **2007**, *282*, 11885–11892. [[CrossRef](#)] [[PubMed](#)]
75. Yewdall, N.A.; Venugopal, H.; Desfosses, A.; Abrishami, V.; Yosaatmadja, Y.; Hampton, M.B.; Gerrard, J.A.; Goldstone, D.C.; Mitra, A.K.; Radjainia, M. Structures of human peroxiredoxin 3 suggest self-chaperoning assembly that maintains catalytic state. *Structure* **2016**, *24*, 1120–1129. [[CrossRef](#)]
76. Poynton, R.A.; Peskin, A.V.; Haynes, A.C.; Lowther, W.T.; Hampton, M.B.; Winterbourn, C.C. Kinetic analysis of structural influences on the susceptibility of peroxiredoxins 2 and 3 to hyperoxidation. *Biochem. J.* **2016**, *473*, 411–421. [[CrossRef](#)] [[PubMed](#)]
77. Shi, L.; Palleros, D.R.; Fink, A.L. Protein conformational changes induced by 1,1'-bis(4-anilino-5-naphthalenesulfonic acid): Preferential binding to the molten globule of DnaK. *Biochemistry* **1994**, *33*, 7536–7546. [[CrossRef](#)] [[PubMed](#)]
78. Jencks, W.P. Binding energy, specificity, and enzymic catalysis: The circe effect. *Adv. Enzymol. Relat. Areas Mol. Biol.* **1975**, *43*, 219–410. [[CrossRef](#)] [[PubMed](#)]
79. Mulholland, A.J. Dispelling the effects of a sorceress in enzyme catalysis. *Proc. Natl. Acad. Sci. USA* **2016**, *113*, 2328–2330. [[CrossRef](#)] [[PubMed](#)]

80. Trujillo, M.; Clippe, A.; Manta, B.; Ferrer-Sueta, G.; Smeets, A.; Declercq, J.-P.; Knoop, B.; Radi, R. Pre-steady state kinetic characterization of human peroxiredoxin 5: Taking advantage of Trp84 fluorescence increase upon oxidation. *Arch. Biochem. Biophys.* **2007**, *467*, 95–106. [[CrossRef](#)] [[PubMed](#)]
81. De Simoni, S.; Linard, D.; Hermans, E.; Knoop, B.; Goemaere, J. Mitochondrial peroxiredoxin-5 as potential modulator of mitochondria-ER crosstalk in MPP<sup>+</sup>-induced cell death. *J. Neurochem.* **2013**, *125*, 473–485. [[CrossRef](#)] [[PubMed](#)]
82. Quijano, C.; Castro, L.; Peluffo, G.; Valez, V.; Radi, R. Enhanced mitochondrial superoxide in hyperglycemic endothelial cells: Direct measurements and formation of hydrogen peroxide and peroxynitrite. *Am. J. Physiol. Heart Circ. Physiol.* **2007**, *293*, H3404–H3414. [[CrossRef](#)] [[PubMed](#)]
83. Antunes, F.; Salvador, A.; Marinho, H.S.; Alves, R.; Pinto, R.E. Lipid peroxidation in mitochondrial inner membranes. I. An integrative kinetic model. *Free Radic. Biol. Med.* **1996**, *21*, 917–943. [[CrossRef](#)] [[PubMed](#)]
84. Noh, Y.H.; Baek, J.Y.; Jeong, W.; Rhee, S.G.; Chang, T.-S. Sulfiredoxin translocation into mitochondria plays a crucial role in reducing hyperoxidized peroxiredoxin III. *J. Biol. Chem.* **2009**, *284*, 8470–8477. [[CrossRef](#)] [[PubMed](#)]
85. Li, X.; Lu, D.; He, F.; Zhou, H.; Liu, Q.; Wang, Y.; Shao, C.; Gong, Y. Cullin 4B protein ubiquitin ligase targets peroxiredoxin III for degradation. *J. Biol. Chem.* **2011**, *286*, 32344–32354. [[CrossRef](#)]
86. Belikova, N.A.; Tyurina, Y.Y.; Borisenko, G.; Tyurin, V.; Samhan Arias, A.K.; Yanamala, N.; Furtmüller, P.G.; Klein-Seetharaman, J.; Obinger, C.; Kagan, V.E. Heterolytic reduction of fatty acid hydroperoxides by cytochrome c/cardiolipin complexes: Antioxidant function in mitochondria. *J. Am. Chem. Soc.* **2009**, *131*, 11288–11289. [[CrossRef](#)]
87. Khailova, L.S.; Prikhodko, E.A.; Dedukhova, V.I.; Mokhova, E.N.; Popov, V.N.; Skulachev, V.P. Participation of ATP/ADP antiporter in oleate-and oleate hydroperoxide-induced uncoupling suppressed by GDP and carboxyatractylate. *Biochim. Et Biophys. Acta (BBA)-Bioenerg.* **2006**, *1757*, 1324–1329. [[CrossRef](#)]
88. Jabůrek, M.; Miyamoto, S.; Di Mascio, P.; Garlid, K.D.; Ježek, P. Hydroperoxy fatty acid cycling mediated by mitochondrial uncoupling protein UCP2. *J. Biol. Chem.* **2004**, *279*, 53097–53102. [[CrossRef](#)]
89. De Simoni, S.; Goemaere, J.; Knoop, B. Silencing of peroxiredoxin 3 and peroxiredoxin 5 reveals the role of mitochondrial peroxiredoxins in the protection of human neuroblastoma SH-SY5Y cells toward MPP<sup>+</sup>. *Neurosci. Lett.* **2008**, *433*, 219–224. [[CrossRef](#)]
90. Portillo, S. Peroxirredoxinas: Eficientes Reductoras de Peróxidos y Eficientemente Reducidas. Función de los Aminoácidos Conservados en Ambas Reacciones. Ph.D. Thesis, Universidad de la República, Montevideo, Uruguay, 2018.
91. Arteel, G.E.; Briviba, K.; Sies, H. Protection against peroxynitrite. *FEBS Lett.* **1999**, *445*, 226–230. [[CrossRef](#)] [[PubMed](#)]
92. Bae, S.H.; Woo, H.A.; Sung, S.H.; Lee, H.E.; Lee, S.K.; Kil, I.S.; Rhee, S.G. Induction of sulfiredoxin via an Nrf2-dependent pathway and hyperoxidation of peroxiredoxin III in the lungs of mice exposed to hyperoxia. *Antioxid. Redox Signal.* **2009**, *11*, 937–948. [[CrossRef](#)]
93. Collins, J.A.; Wood, S.T.; Nelson, K.J.; Rowe, M.A.; Carlson, C.S.; Chubinskaya, S.; Poole, L.B.; Furdulj, C.M.; Loeser, R.F. Oxidative stress promotes peroxiredoxin hyperoxidation and attenuates pro-survival signaling in aging chondrocytes. *J. Biol. Chem.* **2016**, *291*, 6641–6654. [[CrossRef](#)] [[PubMed](#)]
94. Kameritsch, P.; Singer, M.; Nuernbergk, C.; Rios, N.; Reyes, A.M.; Schmidt, K.; Kirsch, J.; Schneider, H.; Müller, S.; Pogoda, K. The mitochondrial thioredoxin reductase system (TrxR2) in vascular endothelium controls peroxynitrite levels and tissue integrity. *Proc. Natl. Acad. Sci. USA* **2021**, *118*, e1921828118. [[CrossRef](#)] [[PubMed](#)]
95. Dalla Rizza, J.; Randall, L.M.; Santos, J.; Ferrer-Sueta, G.; Denicola, A. Differential parameters between cytosolic 2-Cys peroxiredoxins, PRDX1 and PRDX2. *Protein Sci.* **2019**, *28*, 191–201. [[CrossRef](#)] [[PubMed](#)]
96. Peskin, A.V.; Dickerhof, N.; Poynton, R.A.; Paton, L.N.; Pace, P.E.; Hampton, M.B.; Winterbourn, C.C. Hyperoxidation of peroxiredoxins 2 and 3: Rate constants for the reactions of the sulfenic acid of the peroxidatic cysteine. *J. Biol. Chem.* **2013**, *288*, 14170–14177. [[CrossRef](#)]
97. Wood, Z.A.; Poole, L.B.; Karplus, P.A. Peroxiredoxin evolution and the regulation of hydrogen peroxide signaling. *Science* **2003**, *300*, 650–653. [[CrossRef](#)]
98. Zeida, A.; Trujillo, M.; Ferrer-Sueta, G.; Denicola, A.; Estrin, D.A.; Radi, R. Catalysis of peroxide reduction by fast reacting protein thiols: Focus review. *Chem. Rev.* **2019**, *119*, 10829–10855. [[CrossRef](#)] [[PubMed](#)]
99. Talwar, D.; Dick, T.P. Thiol peroxidase-based redox relays. In *Redox Chemistry and Biology of Thiols*; Elsevier: Amsterdam, The Netherlands, 2022; pp. 307–320.
100. Cox, A.G.; Winterbourn, C.C.; Hampton, M.B. Measuring the redox state of cellular peroxiredoxins by immunoblotting. In *Methods in Enzymology*; Elsevier: Amsterdam, The Netherlands, 2010; Volume 474, pp. 51–66.
101. Watabe, S.; Kohno, H.; Kouyama, H.; Hiroi, T.; Yago, N.; Nakazawa, T. Purification and characterization of a substrate protein for mitochondrial ATP-dependent protease in bovine adrenal cortex. *J. Biochem.* **1994**, *115*, 648–654. [[CrossRef](#)] [[PubMed](#)]
102. Nesmachnow, S.; Iturriaga, S. Cluster-UY Collaborative Scientific High Performance Computing in Uruguay. In *Supercomputing. Communications in Computer and Information Science*; Torres, M., Klapp, J., Eds.; Springer: Mexico City, Mexico, 2019; Volume 1151, pp. 188–202.

**Disclaimer/Publisher’s Note:** The statements, opinions and data contained in all publications are solely those of the individual author(s) and contributor(s) and not of MDPI and/or the editor(s). MDPI and/or the editor(s) disclaim responsibility for any injury to people or property resulting from any ideas, methods, instructions or products referred to in the content.